Agricultural and Forest Meteorology 339 (2023) 109560

Contents lists available at ScienceDirect

Agricultural and Forest Meteorology

journal homepage: www.elsevier.com/locate/agrformet

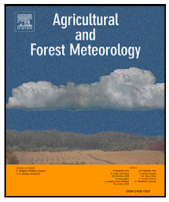

Evapotranspiration regulates leaf temperature and respiration in dryland vegetation

Christopher L. Kibler [a,*], Anna T. Trugman [a,b], Dar A. Roberts [a,b], Christopher J. Still [c], Russell L. Scott [d], Kelly K. Caylor [a,b,e], John C. Stella [f], Michael Bliss Singer [b,g,h]

[a] Department of Geography, University of California, Santa Barbara, Santa Barbara, CA, USA
[b] Earth Research Institute, University of California, Santa Barbara, Santa Barbara, CA, USA
[c] Department of Forest Ecosystems and Society, Oregon State University, Corvallis, OR, USA
[d] Southwest Watershed Research Center, USDA Agricultural Research Service, Tuscon, AZ, USA
[e] Bren School of Environmental Science and Management, University of California, Santa Barbara, Santa Barbara, CA, USA
[f] Department of Sustainable Resources Management, State University of New York College of Environmental Science and Forestry, Syracuse, NY, USA
[g] School of Earth and Environmental Sciences, Cardiff University, Cardiff, United Kingdom
[h] Water Research Institute, Cardiff University, Cardiff, United Kingdom

ARTICLE INFO

Dataset link: Manuscript code and data (Original data)

Keywords:
Carbon cycling
Ecohydrology
Eddy covariance
Evaporative cooling
Thermal remote sensing
Thermoregulation

ABSTRACT

Evapotranspiration regulates energy flux partitioning at the leaf surface, which in turn regulates leaf temperature. However, the mechanistic relationship between evapotranspiration and leaf temperature remains poorly constrained. In this study, we present a novel mechanistic model to predict leaf temperature as a linearized function of the evaporative fraction. The model is validated using measurements from infrared radiometers mounted on two flux towers in Arizona, USA, which measure canopies of *Prosopis velutina* with contrasting water availability. Both the observations and model predictions reveal that leaf temperature equilibrates with air temperature when latent heat flux consumes all of the energy incident on the leaf surface. Leaf temperature exceeds air temperature when there is a net input of energy into the leaf tissue. The flux tower observations revealed that evaporative cooling reduced canopy leaf temperature by *ca.* 1–5 °C, depending on water availability. Evaporative cooling also enhanced net carbon uptake by reducing leaf respiration by *ca.* 15% in the middle of the growing season. The regulation of leaf temperature by evapotranspiration and the resulting impact on net carbon uptake represents an important link between plant water and carbon cycles that has received little attention in literature. The model presented here provides a mechanistic framework to quantify leaf evaporative cooling and examine its impacts on plant physiological function.

1. Introduction

Leaves serve as a critical nexus between water, energy, and carbon fluxes in terrestrial ecosystems, and leaf temperature (T_L) plays an important role in regulating the rates of mass and energy fluxes at the leaf surface (Still et al., 2021; Vinod et al., 2022). T_L directly influences several physical processes that drive mass and energy exchange, including leaf-to-air vapor pressure deficit (VPD; Grossiord et al., 2020), thermal conductance and emittance (Jones, 2014), net photosynthetic assimilation (Medlyn et al., 2002), and leaf respiration (R_L; Heskel et al., 2016). High values of T_L can also cause thermal stress and damage to leaf biochemical systems, which may permanently inhibit leaf physiologic function (O'Sullivan et al., 2017). T_L is thus a critical variable that regulates several aspects of terrestrial ecosystem function, and it is important to constrain the drivers of T_L to better predict the sensitivity of terrestrial ecosystems to anthropogenic climate change.

Generally speaking, T_L is regulated by environmental conditions and energy fluxes at the leaf surface. Empirical observations have demonstrated that T_L is often close to air temperature (T_a), but the mechanistic relationship between T_L and T_a remains poorly constrained. Some studies have argued that leaves exhibit limited homeothermy, whereby the slope of the relationship between T_L and T_a is less than 1 (Michaletz et al., 2015, 2016; Blonder and Michaletz, 2018; Cook et al., 2021). Other studies have argued that leaves exhibit megathermy, whereby the slope of the relationship between T_L and T_a is greater than 1 (Salisbury and Spomer, 1964; Pau et al., 2018; Still et al., 2019b, 2022). Observations where $T_L \cong T_a$ (i.e., poikilothermy) have also been reported (Drake et al., 2020; Miller et al., 2021; Uni et al.,

* Corresponding author.
E-mail address: kibler@ucsb.edu (C.L. Kibler).

https://doi.org/10.1016/j.agrformet.2023.109560
Received 11 November 2022; Received in revised form 16 March 2023; Accepted 6 June 2023

2022). The terminology for leaf thermal regimes follows the convention described by Cavaleri (2020). In practice, T_L observations are often normalized by T_a (i.e., $T_L - T_a$) to control for environmental variability and analyze other drivers of T_L.

Surface energy flux partitioning between latent (λE) and sensible (H) heat flux also plays an important role in regulating T_L. Surface energy balance must be preserved at the leaf scale, so leaf-level λE consumes energy that would otherwise increase T_L. Surface energy flux partitioning can be quantified using the evaporative fraction (f_E), which measures the proportion of available energy (Q_a) that is consumed by λE:

$$f_E = \frac{\lambda E}{Q_a} \tag{1}$$

Thus, there is a direct physical relationship between f_E and T_L, which results in evaporative cooling of the leaf surface.

Evaporative cooling has important functional implications for plant carbon cycling and leaf physiologic function, particularly in hot and dry ecosystems (Hultine et al., 2020; Uni et al., 2022). Photosynthetic assimilation of carbon is highly dependent on T_L at the leaf scale (Medlyn et al., 2002). Maintaining lower T_L also reduces R_L (Heskel et al., 2016; Mathias and Trugman, 2022) and can prevent thermal damage to leaves (O'Sullivan et al., 2017). Indeed, several recent studies have speculated that plants may decouple photosynthesis and transpiration during extreme heat waves to maintain high levels of λE, which keeps T_L below critical thresholds that would result in damage to the leaf tissue (Drake et al., 2018; Krich et al., 2022; *cf.* De Kauwe et al., 2019). Likewise, water availability for evaporative cooling may limit the distributions of some plant species in dryland ecosystems when they cannot maintain physiologic function at ambient temperatures (Hultine et al., 2020). Improving mechanistic models of T_L will enhance our understanding of the feedbacks between water, energy, and carbon fluxes at the leaf surface and improve our ability to predict shifts in ecosystem function under anthropogenic climate change. It will also improve our ability to map ecosystem water fluxes at broad spatial scales using thermal remote sensing data (Mallick et al., 2022).

Many models predict T_L or $T_L - T_a$ by combining energy balance theory with the Penman-Monteith equation (e.g., Monteith and Unsworth, 2013). However, implementing these models requires empirical assumptions about stomatal conductance, which is difficult to constrain. Here, we present an alternate modeling framework that predicts T_L as a linearized function of f_E. Our mechanistic model requires fewer surface parameters than previous formulations, which improves our ability to isolate and examine the environmental variables that drive T_L. The simplified model also yields fundamental insights into the relationship between T_L and T_a under varying environmental conditions, and the resulting impacts on plant physiologic function.

The paper is organized as follows. First, we present the new model. Then, we validate the model predictions using T_L measurements from infrared radiometers mounted on two flux towers in Arizona, USA, which measure stands of *Prosopis velutina* with contrasting water availability. We also examine the environmental variables that are most important for predicting T_L in the observational data set. Finally, we force the model with flux tower measurements to estimate the change in R_L that is attributable to evaporative cooling of the leaf surface, which may reveal an important link between evaporative cooling and net carbon uptake. In doing so, we address the following research questions:

1. How sensitive is T_L to changes in surface energy flux partitioning between λE and H?
2. Which environmental variables directly regulate T_L? Which of those variables is most important for regulating T_L in dryland ecosystems?
3. How much is R_L reduced by evaporative cooling of the leaf surface?

2. Methods

2.1. Leaf temperature model

Steady-state surface energy balance can be modeled as the difference between Q_a, H, and λE:

$$Q_a - H - \lambda E = 0 \tag{2}$$

When modeling the energy balance of individual leaves, the Q_a term is equivalent to leaf-level net radiation (R_n), which is the sum of downwelling (↓) and upwelling (↑) shortwave (SW) and longwave (LW) radiation fluxes:

$$R_n = SW\downarrow - SW\uparrow + LW\downarrow - LW\uparrow \tag{3}$$

The $LW\uparrow$ term can be calculated as a function of T_L measured in K:

$$LW\uparrow = k\varepsilon_L \sigma T_L^4 \tag{4}$$

where ε_L is leaf emissivity ($\varepsilon_L = 0.98$), σ is the Stefan–Boltzmann constant (5.67 ×10^{-8} W m^{-2} K^{-4}), and k is a coefficient that indicates whether it is a one-sided ($k = 1$) or two-sided ($k = 2$) leaf model. The H term in Eq. (2) can be calculated as:

$$H = k\frac{\rho c_p (T_L - T_a)}{r_H} \tag{5}$$

where ρ is air density, c_p is the specific heat of air, and r_H is the aerodynamic resistance to H. We combined Eqs. (1), (2), and (5) and rearranged to produce a novel linearized equation for $T_L - T_a$:

$$\begin{aligned} T_L - T_a &= \frac{Q_a r_H}{k\rho c_p}\left(1 - f_E\right) \\ &= \frac{Q_a r_H}{k\rho c_p} - \frac{Q_a r_H}{k\rho c_p} f_E \end{aligned} \tag{6}$$

The expanded version of Eq. (6) contains two additive terms: a radiative heating term that is proportional to Q_a and an evaporative cooling term that is proportional to f_E. Importantly, Eq. (6) reveals that $T_L - T_a$ is a linear function of f_E and that the slope and intercept are functions of Q_a and r_H. Because the slope and intercept negate each other (i.e., slope = intercept × -1), $T_L - T_a = 0$ °C when $f_E = 1$, which reveals that T_L converges at T_a when λE consumes all of the energy incident on the leaf surface. It follows that:

$$T_L = T_a + \frac{Q_a r_H}{k\rho c_p} - \frac{Q_a r_H}{k\rho c_p} f_E \tag{7}$$

Eq. (7) provides a framework to examine the competing roles of T_a, radiative heating, and evaporative cooling in regulating T_L. It also provides a framework to examine the resulting impacts on plant physiologic function.

It is worth noting that T_L appears on both sides of Eq. (7) because T_L regulates R_n and thus Q_a (i.e., Eq. (4)). If R_n is not measured directly, Eq. (7) can be solved numerically, as is discussed below in Section 2.3.7. Alternatively, the R_n term can be approximated using isothermal net radiation ($R_{n,i}$) following Jones (2014):

$$R_{n,i} = SW\downarrow - SW\uparrow + \varepsilon_L LW\downarrow - k\varepsilon_L \sigma T_a^4 \tag{8}$$

We used direct measurements of R_n throughout our analysis, except as noted in Section 2.3.7.

2.2. Leaf temperature sensitivity analysis

We modeled the sensitivity of $T_L - T_a$ to environmental drivers by forcing Eq. (6) with simulated values of Q_a (250, 500, and 750 Wm^{-2}), r_H (1, 10, 20, 30, and 40 sm^{-1}), and f_E (0-1). The ρ term was held constant at 1.006 kg m^{-3}, and the c_p term was held constant at 1010 J K^{-1} kg^{-1}, which are representative values for the study area. A one-sided model ($k = 1$) was used to facilitate intercomparison with subsequent analyses.

2.3. Flux tower observations

We compared the modeled sensitivities from Eq. (6) to measurements from two eddy covariance flux towers in Arizona, USA, where T_L was measured by infrared radiometers mounted on the towers. The infrared radiometers measured the average temperature of many leaves on the outside of the *P. velutina* canopies, so we use the term T_c to describe the radiometer measurements of "canopy-scale leaf temperature" following (Still et al., 2021). However, we generally assume that $T_c \cong T_L$, and we use T_c and T_L interchangeably. The flux tower data set contains 17 site-years of growing season measurements under varying environmental conditions. We also used the flux tower data to analyze the environmental drivers of T_c and to quantify the impact of T_c on R_L.

The T_c measurements by the infrared radiometers represent leaves on the outside of a single *P. velutina* canopy, while the eddy covariance measurements represent the average fluxes within the fetch of the sensors (*ca.* 50–200 m). We acknowledge the scale mismatch between the canopy-scale T_c measurements and the fetch-scale flux measurements, but we contend that novel insights can still be gleaned from the measurements using a "big leaf" assumption, whereby the entire fetch is assumed to behave like a single leaf in order to link leaf-scale theoretical models with canopy-scale measurements (e.g., Sellers et al., 1992; Amthor, 1994). In this context, Eq. (7) can be used to predict the average surface temperature of an entire canopy or stand. Canopy-scale processes are arguably more important than leaf-scale processes for understanding terrestrial ecosystem function, but they are also more difficult to constrain (Bonan, 2016). The temperature and fluxes of individual leaves can be measured using *in situ* sensors, but they may not be representative of the canopy as a whole (Miller et al., 2021; Vinod et al., 2022). We believe that the big leaf assumption is a reasonable approach to glean insights into the theoretical drivers of canopy-scale processes. To connect the leaf-scale theoretical model with the canopy-scale measurements, we included a ground heat flux (G) term when calculating Q_a, such that:

$$Q_a = R_n - G \tag{9}$$

Eq. (9) helps control for the loss of available energy through the bottom of the canopy. We also used a one-sided model ($k = 1$) for all analyses.

2.3.1. Study sites

We analyzed data from two flux towers located in stands of *P. velutina* in southeastern Arizona, USA. Southeastern Arizona has a semi-arid climate with monsoonal precipitation that is delivered in brief, spatially restricted storms that dominate total annual rainfall and runoff (Thomas and Pool, 2006; Singer and Michaelides, 2017). The summer growing season encompasses both the driest and wettest parts of the year. The first part of the growing season is very dry, but ecosystems receive intense precipitation after the onset of the monsoon around early July. The monsoonal precipitation and accompanying humidity typically decrease after August, but generally remain above pre-monsoon levels through the end of the growing season (Higgins et al., 1997). The two stands that we analyzed have contrasting physiographic positions resulting in differences in plant water availability, particularly during the dry months before the onset of the monsoon. The differences in water availability create ideal conditions for a natural experiment to quantify the sensitivity of T_c to λE and environmental conditions, while holding regional climatic variables relatively constant.

The first flux tower is in a riparian woodland approximately 16 km northeast of Sierra Vista, Arizona (31.6637° N, 110.1777° W). The riparian woodland is located on an old alluvial terrace above the San Pedro River, where the depth to groundwater is approximately 10 m (Sabathier et al., 2021). The flux tower is located *ca.* 225 m from the river channel, and the alluvial terrace is *ca.* 10 m above the river channel, so we assume that evaporation from the river channel does not affect the λE measurements. The mean summer air temperature is 25 °C and the mean annual precipitation is 319 mm (PRISM Climate Group, 2021; Huntington et al., 2017). The woodland is dominated by a canopy of *P. velutina* (canopy cover ~70%) with a mean height of 7 m and a maximum height of 10 m. Leaf emergence for the deciduous *P. velutina* trees typically occurs in April, and plant hydraulic function increases in late May. The understory is dominated by the perennial grass *Sporobolus wrightii* but annual forbs and herbs are common during the summer monsoon season (Scott et al., 2004). Rooting depths of *P. velutina* can exceed 10 m (Stromberg, 2013), and the pre-monsoon fluxes reveal that overstory vegetation accesses groundwater. Because groundwater provides a stable source of water that is somewhat decoupled from the local precipitation regime, evapotranspiration (ET) consistently exceeds precipitation on an annual basis (Missik et al., 2021; Scott et al., 2021). Groundwater is an important water source for maintaining vegetation structure and function in many dryland riparian plant communities (Kibler et al., 2021). The understory vegetation has a maximum rooting depth of 2–3 m, so it does not have access to groundwater and is dependent on water inputs from local precipitation (Scott et al., 2004).

The second flux tower is in an upland savanna at the Santa Rita Experimental Range, approximately 45 km south of Tucson, Arizona (31.8214° N, 110.8661° W). The site is a semi-desert grassland that has been encroached by *P. velutina*. The mean summer air temperature is 26 °C and the mean annual precipitation is 368 mm (PRISM Climate Group, 2021; Huntington et al., 2017). Scott et al. (2009) reported that the *P. velutina* canopy ranges in height from 0.25 to 6 m (mean height 2.5 m) and covers ~35% of the ground area. Leaf emergence for *P. velutina* typically occurs in April (Seyednasrollah et al., 2019). The *P. velutina* plants at the upland savanna likely had lower leaf area index and smaller average leaf size than those at the riparian woodland (Stromberg et al., 1993). Perennial grasses, forbs, and subshrubs cover ~22% of the ground area (Scott et al., 2009). Depth to groundwater exceeds 100 m, so the overstory and understory vegetation do not have access to groundwater and are dependent on water inputs from local precipitation.

Both flux towers contain an array of eddy covariance, meteorological, and soil sensors, along with infrared radiometers (IRT-P, Apogee Instruments, Logan, UT) pointed 45° off-nadir at the *P. velutina* canopies. This study primarily relied on flux measurements of λE, H, R_n, G, SW↓, SW↑, and LW↓; meteorological measurements of T_a, wind speed (u), and relative humidity (RH); measurements of soil temperature (T_s) and soil water content (SWC); and T_c measurements from the infrared radiometers. In the riparian woodland, λE and H were measured at 14 m. G was quantified for the surface using soil heat flux plate measurements at 5 cm depth along with the change in heat storage from 0–5 cm depth. Canopy-level T_a, u, and RH were measured at 8 m. T_s was measured at 5 cm depth and SWC was measured at 22.5 cm depth. The infrared radiometer was mounted at 10 m. A four-component net radiometer measured individual SW↓, SW↑, LW↑, and LW↓ fluxes from 2001–2003, but it was replaced by a two-channel SW and LW net radiometer from 2004–2006. The four-channel radiometer was mounted at 14 m, and the sensors for the two-channel radiometer were mounted at 10 m and 14 m. In the upland savanna, λE and H were measured at 7.8 m; SW↓, SW↑, LW↑, and LW↓ were measured at 7.1 m; and G was quantified for the surface. Canopy-level T_a and RH were measured at 2 m. Canopy-level u was measured at 3.5 m. T_s was measured at 5 cm depth and SWC was measured at 20 cm depth. The infrared radiometer was mounted at 7 m. Atmospheric transmittance and emittance were assumed to have a negligible impact on the radiometer measurements over the short distances (*ca.* 5 m) between the radiometers and the canopies (Aubrecht et al., 2016). We also assumed that the differences in T_a between the meteorological sensors and the canopies were negligible, given that the T_a sensors were at approximately the same heights as the measured leaves. All flux tower data were acquired from Ameriflux (sites US-CMW and US-SRM, respectively). See Scott (2021a,b) and Scott et al.

(2004, 2009) for additional details about the collection and processing of the flux tower data.

Several criteria were used to filter the half-hourly flux tower measurements:

- growing season observations between May and September
- daytime observations between 8:00 and 16:00 local time
- removed days with any measured precipitation and the day after any measured precipitation
- observations with friction velocity (u_*) > 0.2

We also removed years that did not have complete records of growing season measurements and years where there were apparent shifts in the infrared radiometer view angle due to a loose mounting bracket, as evidenced by sudden changes in the relationship between T_c and T_s at 5 cm depth. Based on these criteria, two site-years of data were removed for the riparian woodland (2007 and 2008), and four site-years of data were removed for the upland savanna (2014, 2015, 2020, and 2021). The resulting data set contained six site-years of data for the riparian woodland (2001–2006) and eleven site-years of data for the upland savanna (2007–2019, excluding 2014 and 2015). The R_L analysis relied on individual measurements of SW↓, SW↑, and LW↓ fluxes, which were only available from 2001–2003 at the riparian woodland. They were available for all years at the upland savanna. The flux tower measurements were used to force Eq. (7) and analyze the sensitivity of T_c to λE and environmental conditions. All of the other terms in Eq. (7) can be directly derived from the flux tower measurements, except for r_H.

2.3.2. Resistance to sensible heat flux

Following Young et al. (2021), the canopy-scale r_H is the sum of the resistance to momentum transfer (r_{am}) and the excess resistance (r_{bh}):

$$r_H = r_{am} + r_{bh} \tag{10}$$

The r_{am} term can be estimated as a function of u and the friction velocity (u_*):

$$r_{am} = \frac{u}{u_*^2} \tag{11}$$

The r_{bh} term is a function of the roughness lengths for momentum (z_{0m}) and heat (z_{0h}) as well as stability functions for momentum (ψ_m) and heat (ψ_h) exchange:

$$r_{bh} = \frac{1}{\kappa u_*}\left[ln\left(\frac{z_{0m}}{z_{0h}}\right) - \psi_h + \psi_m\right] \tag{12}$$

where κ is the Von Kármá n constant (κ = 0.41). Eq. (8) can be simplified to ignore the stability functions, which have a negligible impact on the predicted values of r_{bh} at a canopy scale (Young et al., 2021):

$$r_{bh} = \frac{1}{\kappa u_*} ln\left(\frac{z_{0m}}{z_{0h}}\right) \tag{13}$$

The z_{0m} and z_{0h} terms are often represented by the parameter kB^{-1} such that:

$$kB^{-1} = ln\left(\frac{z_{0m}}{z_{0h}}\right) \tag{14}$$

$$r_{bh} = \frac{1}{\kappa u_*} kB^{-1} \tag{15}$$

At an ecosystem scale, the parameter kB^{-1} varies as a function of land cover, leaf area, vegetation structure, and environmental conditions (Yang and Friedl, 2003). Various empirical formulations for kB^{-1} have been developed. We estimated kB^{-1} as an empirical function of u_* following (Thom, 1972), which yielded the most parsimonious predictions of r_H out of 12 formulas described by Verhoef et al. (1997) and Hong et al. (2012). The comparison of the formulas is described in the Supplementary Materials.

$$kB^{-1} = 1.35\kappa(100u_*)^{1/3} \tag{16}$$

2.3.3. Model validation

The flux tower measurements were used to validate the model described in Eq. (7). We compared the T_c measurements from the infrared radiometers to T_c predictions that were generated by forcing Eq. (7) with concurrent flux tower measurements. The MAE, R^2, slope, and bias were used to quantify the model performance at each site.

2.3.4. Energy balance closure

The model presented in Eq. (7) assumes energy balance closure. However, energy balance closure is rarely achieved in eddy covariance measurements due to systematic sensor errors, differences in the spatial footprints of individual sensors, advective fluxes, and a variety of other factors (Stoy et al., 2013; Mauder et al., 2020). The energy balance closure ratio (C) can be calculated as:

$$C = \frac{\lambda E + H}{Q_a} \tag{17}$$

We calculated C for the half-hourly flux measurements using Eq. (17).

We quantified the sensitivity of the T_c predictions to C by forcing closure in the flux measurements and then comparing the T_c predictions from the forced and unforced values. While forcing energy balance closure is often not recommended for eddy covariance analyses (e.g., Scott, 2010), comparing the different T_c predictions enabled us to quantify the model error that might be attributable to the lack of energy balance closure. Energy balance closure was forced by assuming that the λE and H were measured correctly and adjusting the value of Q_a. Energy balance closure can also be forced by assuming that Q_a was measured correctly and adjusting the values of λE and H (Twine et al., 2000; Knauer et al., 2018). However, the H term is not explicitly represented in Eq. (7). Energy balance closure was forced by setting Q_a equal to the sum of the turbulent fluxes:

$$Q_{a,f} = \lambda E + H \tag{18}$$

where the subscript f denotes that the value was adjusted to force energy balance closure. Eq. (7) was forced with $Q_{a,f}$ to generate a new set of T_c predictions. All other model forcings remained unchanged. We compared the two sets of T_c predictions to estimate the model error that might be attributable to the lack of energy balance closure.

2.3.5. T/ET partitioning

The model presented in Eq. (7) also assumes that all λE is attributable to leaf transpiration (T). However, eddy covariance measurements are collected at a stand scale, and soil evaporation (E) may also contribute to the λE signal. The ratio of T/ET can be used to quantify the extent to which the λE signal is attributable to T. Several methods have been proposed to partition T and E in eddy covariance measurements (Stoy et al., 2019). We reanalyzed data from Scott et al. (2021) and Nelson et al. (2020a,b), who partitioned data for the riparian woodland and upland savanna, respectively, using the method proposed by Nelson et al. (2018). We used their daily estimates of T and ET to calculate T/ET for the two sites. The T/ET analysis included all days where there was at least one half-hourly measurement in the filtered eddy covariance data set and an estimate of T/ET from the published data sets. The resulting data set covered years 2005–2006 for the riparian woodland and 2007–2013 for the upland savanna.

2.3.6. Analysis of flux tower measurements

We conducted several analyses to identify the mechanistic basis for the model behavior using the flux tower measurements. We compared the distributions of the $T_c - T_a$ and f_E measurements and calculated the seasonal and diurnal climatology of $T_c - T_a$ at each site. We also produced seasonal and diurnal climatologies for the individual drivers of T_c, including T_a, f_E, r_H, and Q_a. Spearman rank correlation was used to quantify the sensitivity of T_c and $T_c - T_a$ to the individual drivers. The data were grouped by month to assess seasonal changes in the variables that drive T_c and $T_c - T_a$. Spearman rank correlation was also used to

quantify the sensitivity of f_E, r_H, and Q_a to environmental variables measured by the flux towers, which may have an indirect effect on T_c and $T_c - T_a$. The environmental variables include SW↓, VPD, u, and soil water content (SWC). VPD was calculated using the flux tower measurements of T_a and RH following Allen et al. (1998).

2.3.7. Leaf respiration model

We also analyzed the sensitivity of daytime leaf respiration (R_L) to changes in T_c caused by λE variability. Leaf respiration is a complex biochemical process that varies as a function of leaf mass per area, leaf nitrogen and phosphorus concentrations, photosynthetic carboxylation capacity, T_L, and other variables (Atkin et al., 2015). Leaf respiration is also inhibited by sunlight during the daytime (Kok, 1948; Heskel et al., 2013). In practice, R_L is often estimated as an empirical function of T_L (Mathias and Trugman, 2022). We estimated leaf dark respiration ($R_{L,dark}$) following Heskel et al. (2016):

$$R_{L,dark}(T_L) = R_{L,dark}(T_{ref}) * e^{0.1012(T_L - T_{ref}) - 0.0005(T_L^2 - T_{ref}^2)} \quad (19)$$

where T_{ref} is the reference temperature and $R_{L,dark}$ is measured in units of μmol CO_2 $m^{-2}s^{-1}$. The $R_{L,dark}(T_{ref})$ parameter was set to 1.7 μmol CO_2 $m^{-2}s^{-1}$ based on a measurement of *Prosopis glandulosa* by Reich et al. (1998) at a T_{ref} of 25 °C. Leaf light respiration ($R_{L,light}$) was modeled as a function of $R_{L,dark}$ following Way et al. (2015) and Mathias and Trugman (2022):

$$R_{L,light}(T_L) = R_{L,dark}(T_L) * (0.0039 * T_L + 0.6219) \quad (20)$$

Eq. (20) helps control for the light inhibition of R_L, which is not represented in the $R_{L,dark}$ estimates (Way et al., 2015).

We estimated $R_{L,light}$ using two temperature forcings: T_c and modeled canopy temperature with no evaporative cooling ($T_{c,ne}$). We modeled T_c by forcing Eq. (7) with flux tower measurements. The r_H term was calculated using Eqs. (10)–(16). We used modeled rather than measured T_c values to control for any effect of changing sensor calibrations over the multi-annual time series. We modeled $T_{c,ne}$ by setting λE to 0 in Eq. (7). We also calculated Q_a as a function of its component fluxes (Eqs. (3)–(4)) to account for the effect of T_c on $LW\uparrow$. When all terms in Eq. (7) are directly measured, the feedback between T_c and $LW\uparrow$ is implicitly encoded in the flux measurements. However, when combining measured and forced flux values (i.e., by setting λE to 0), the feedback must be explicitly specified in the analytical formulation. The $LW\downarrow$ term must also be multiplied by ε_L. The equation for $T_{c,ne}$ can be written as:

$$T_{c,ne} = T_a + \frac{(SW\downarrow - SW\uparrow + \varepsilon_L LW\downarrow - \varepsilon_L \sigma T_{c,ne}^4 - G) r_H}{\rho c_p} \quad (21)$$

Eq. (21) estimates the temperature of a non-transpiring canopy. The terms of the equation were forced with flux tower measurements. To make Eq. (21) analytically tractable, we rewrote the equation in the form of a quartic function and solved for $T_{c,ne}$ using a numerical solver (NumPy v1.23.3; Harris et al., 2020). Physically unreasonable values where modeled $T_{c,ne}$ was less than modeled T_c were likely due to the lack of energy balance closure and were removed from the analysis.

The difference between the estimates of $R_{L,light}$ using T_c and $T_{c,ne}$ revealed the marginal change in $R_{L,light}$ that is attributable to T_c variability caused by λE (i.e., $\partial R_{L,light}/\partial T_c(\lambda E)$). This framework enabled us to estimate the decrease in daytime R_L caused by evaporative cooling of the leaf surface (ΔR_L).

3. Results

3.1. Leaf temperature model

The mechanistic model of T_L presented in Eq. (7) reveals that there are three drivers of T_L: (1) T_a, (2) a radiative heating term that is proportional to Q_a, and (3) an evaporative cooling term that is proportional to f_E. The model predicts that T_L converges to T_a when λE consumes all of the energy incident on the leaf surface, regardless of environmental conditions (Fig. 1). When $f_E < 1$, $T_L - T_a$ also varies as a function of Q_a and r_H. Importantly, the model predicts that $T_L - T_a \geq 0$ °C under all conditions, although there are environmental conditions when $T_L - T_a$ approaches 0 °C even though $f_E < 1$. Specifically, the model predicts that $T_L - T_a = 0$ °C when $Q_a = 0$ Wm^{-2} or when $r_H = 0$ sm^{-1}, regardless of the value of f_E. The first condition often happens around dawn and dusk, while the second condition is unrealistic in real-world settings (Young et al., 2021).

3.2. Model validation

The model of T_L presented in Eq. (7) was validated by forcing Eq. (7) with flux tower measurements and comparing the T_L predictions to concurrent T_c measurements from infrared radiometers mounted on the flux towers. The T_c measurements represented the average temperature of many leaves on the outside of a *P. velutina* canopy, and we generally assumed that $T_c \cong T_L$. The model yielded strong fits at both study sites (Fig. 2). The predictions for the riparian woodland exhibited a stronger fit (MAE = 2.67 °C). The predictions for the upland savanna exhibited a slightly weaker fit (MAE = 3.42 °C), but the range of observed T_c values was also larger. The model tended to slightly overestimate T_c at both sites (mean bias = 2.53 °C and 1.55 °C, respectively).

3.3. Energy balance closure

We also assessed the impact of energy balance closure on the T_c predictions. The median energy balance closure ratio (C) in the riparian woodland was 0.86 with an interquartile range of [0.75, 0.98]. The median C in the upland savanna was 0.83 with an interquartile range of [0.75, 0.92] (Supplementary Figure 4). Forcing energy balance closure by adjusting the Q_a value reduced the T_c predictions by 1.06 °C in the riparian woodland and 1.64 °C in the upland savanna. The MAE between the two sets of T_c predictions was 1.38 °C in the riparian woodland and 1.8 °C in the upland savanna. The T_c predictions based on $Q_{a,f}$ were more parsimonious than the predictions based on the unforced values when compared to the infrared radiometer measurements at both sites. The R^2 values were 0.89 and 0.7 for the riparian woodland and upland savanna, respectively. The analysis suggests that the overestimation of T_c seen in Fig. 2 is due, in part, to the lack of energy balance closure in the flux data. This is supported by comparing the model prediction error to the C values. In the riparian woodland, the average model prediction error was near 0 °C when $C \approx 1$. When C decreased below 1, the model prediction error increased monotonically. In the upland savanna, the model prediction error also increased as C decreased below 1, although the upland savanna exhibited a less clear trend (Supplementary Figure 5).

3.4. T/ET partitioning

The analysis of T/ET values indicated that the λE signal was dominated by T and not E at both sites (Fig. 3). In the riparian woodland, the median daily T/ET value ranged from 0.87 to 0.92 for each month. In the upland savanna, the median daily T/ET value ranged from 0.72 to 0.8 for each month. The upland savanna exhibited more variability in T/ET values, suggesting that E may have contributed more error to the model predictions at that site. The T/ET values were relatively consistent throughout the growing season and did not exhibit any apparent seasonal trend at either site.

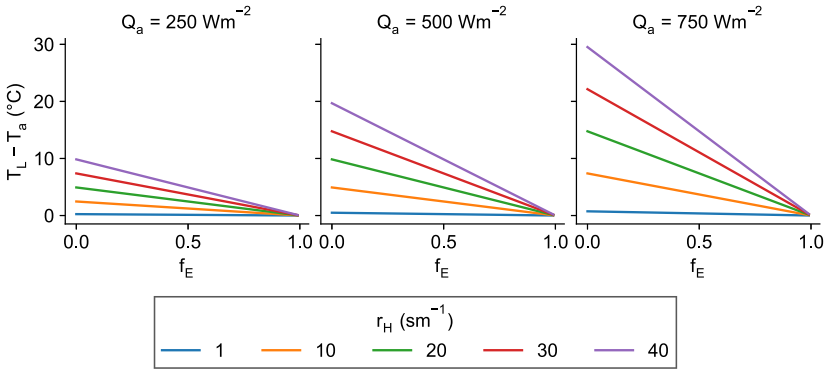

Fig. 1. Predicted values of $T_L - T_a$ from Eq. (6) calculated using different values of available energy (Q_a), evaporative fraction (f_E), and resistance to sensible heat flux (r_H). Air density (ρ) was held constant at 1.006 kg m^{-3}. The specific heat of air (c_p) was held constant at 1010 J K^{-1} kg^{-1}.

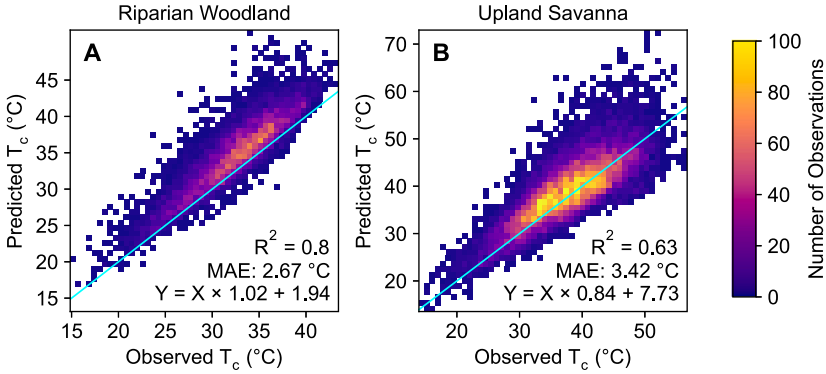

Fig. 2. Model predicted T_c compared to T_c measurements from the infrared radiometers for the riparian woodland (a) and upland savanna (b). The predicted T_c values were calculated by forcing Eq. (7) with flux tower measurements. The blue lines are the 1:1 line. The mean absolute error (MAE) is also indicated. White areas in the plots indicate that there were 0 observations in that portion of the feature space. The color scale saturates when there are more than 100 half-hourly observations in a given portion of the feature space.

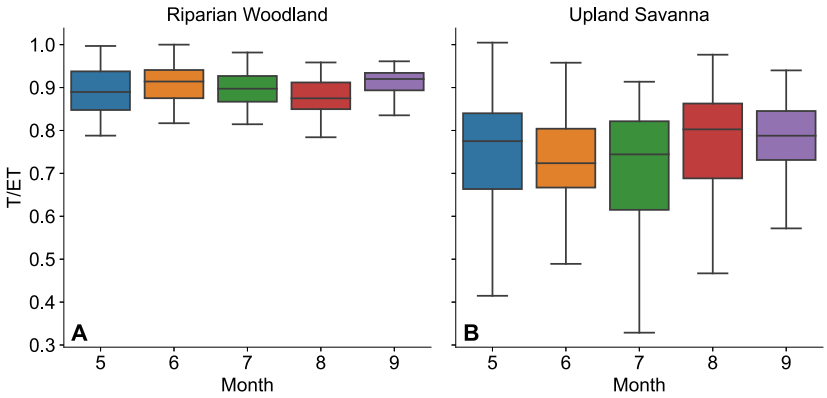

Fig. 3. Boxplots of daily T/ET values in the riparian woodland (a) and upland savanna (b) for each month of the growing season. Outliers are not shown. *Source:* Data are reanalyzed from Scott et al. (2021) and Nelson et al. (2020a,b).

3.5. Flux tower observations

We also analyzed the flux tower observations to characterize the mechanistic basis for the model behavior. In the riparian woodland, $T_c - T_a$ remained close to 0 °C for the entire time series, although $T_c - T_a$ varied both seasonally and diurnally. The mean $T_c - T_a$ value across the entire data set was 1.57 °C (Fig. 4). $T_c - T_a$ values near 0 °C indicate that there was a substantial degree of evaporative cooling in the riparian woodland. Otherwise, T_c would substantially exceed T_a because of energy inputs from solar radiation. The largest $T_c - T_a$ values tended to occur in May when the trees were leafing out and plant hydraulic function was still increasing. The values decreased substantially starting in June (Fig. 5). In May, the average peak value was 4.27 °C, and by June the average peak value decreased to 2.44 °C, with lower peaks occurring in subsequent months. The daily maximum values tended to occur around 11:30 local time.

The upland savanna exhibited similar trends. The mean $T_c - T_a$ value across the entire data set was 6.46 °C (Fig. 4). The largest values tended to occur in the dry months of May and June and decreased substantially starting in July when the summer rainy season began (Fig. 5). In June, the average peak value was 10.59 °C. By August, the average peak value decreased to 5.72 °C. Unlike the riparian woodland, the daily maximum values tended to occur around 13:00 local time.

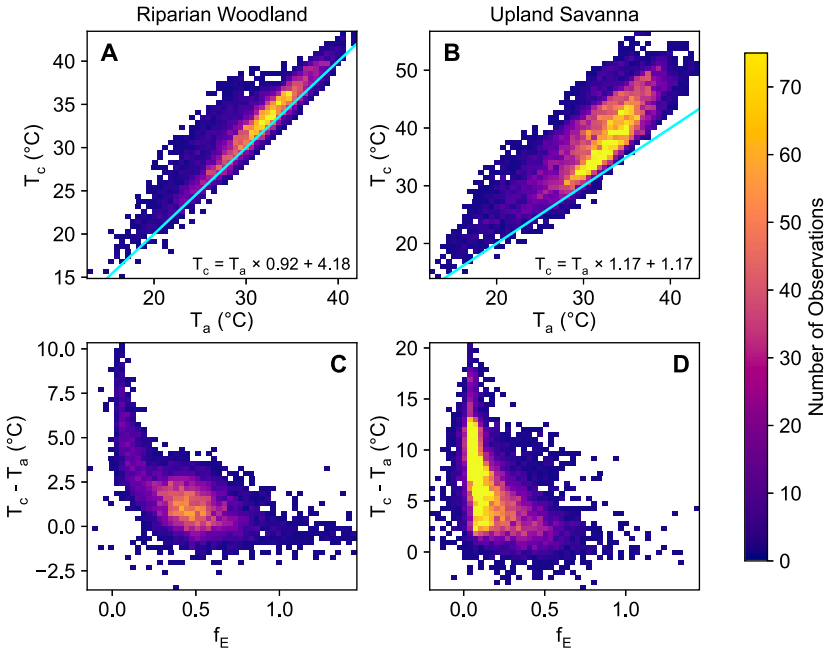

Fig. 4. Energy flux measurements from the riparian woodland (a,c) and upland savanna (b,d) differ in that the riparian woodland has a higher evaporative fraction (f_E) compared to the upland savanna. However, in both systems leaf temperature (T_c) converges to air temperature (T_a) when f_E approaches 1. The plots in the top row (a,b) compare T_a and T_c measurements. The blue lines are the 1:1 line. The plots in the bottom row (b,d) show the relationship between $T_c - T_a$ and f_E. White areas in the plots indicate that there were 0 observations in that portion of the feature space. The color scale saturates when there are more than 75 half-hourly observations in a given portion of the feature space. Some outliers are outside of the plotted range.

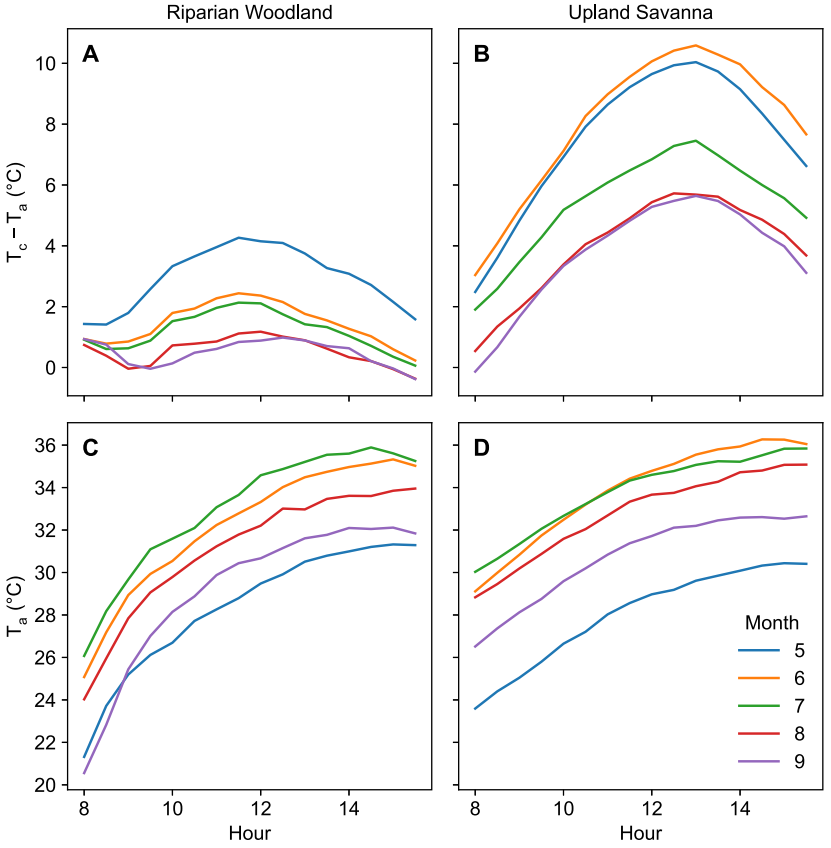

Fig. 5. Diurnal and seasonal climatology of $T_c - T_a$ (a,b) and T_a (c,d) in the riparian woodland (a,c) and upland savanna (b,d). The colored lines represent the mean values for each time of day, grouped by month of the growing season. A comparable figure for f_E, r_H, and Q_a is located in the Supplementary Materials.

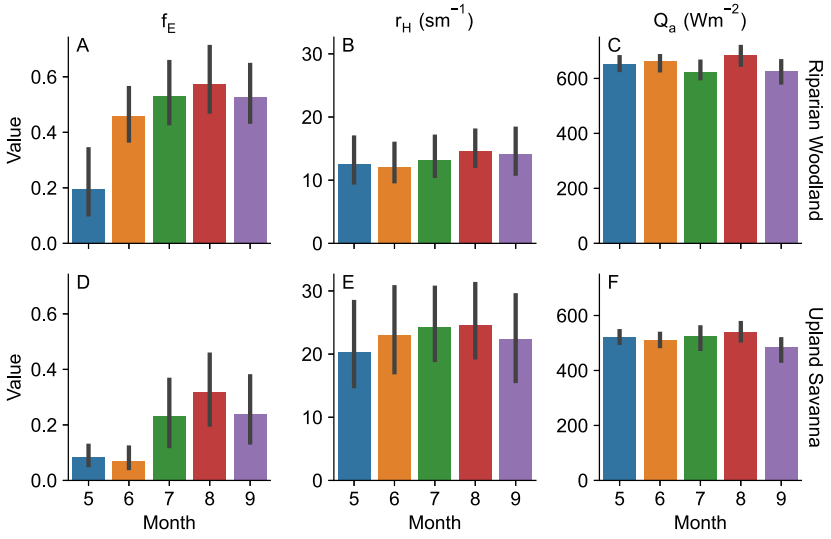

Fig. 6. Seasonal climatology of evaporative fraction (f_E), resistance to sensible heat flux (r_H), and available energy (Q_a) in the riparian woodland (a–c) and upland savanna (d–f). The colored bars represent the median values for each month of the growing season. The black vertical bars represent the interquartile range. The Q_a values are limited to observations from 12:00 local time.

The sensitivity of $T_c - T_a$ to f_E from the flux tower measurements was consistent with the sensitivity predicted by Eq. (6). At both sites, $T_c - T_a$ converged to 0 °C as f_E approached 1 (Fig. 4), which is consistent with the model predictions shown in Fig. 1. When $f_E < 1$, the range and distribution of measured $T_c - T_a$ values was also similar to the modeled values. The $T_c - T_a$ values ranged from −1.24 °C (1st percentile) to 7.61 °C (99th percentile) in the riparian woodland and −0.25 °C (1st percentile) to 16.44 °C (99th percentile) in the upland savanna. The maximum values at both sites occurred when f_E approached 0, consistent with the model predictions. The f_E values for the upland savanna (mean $f_E = 0.15$) were on average lower than the f_E values for the riparian woodland (mean $f_E = 0.46$), which provides a mechanistic explanation for why $T_c - T_a$ was generally greater at the upland savanna than the riparian woodland.

The flux tower measurements exhibited a non-linear relationship between f_E and $T_c - T_a$, especially at the riparian woodland. The model in Eq. (6) predicts a linear relationship between f_E and $T_c - T_a$ when all other variables are held constant. The apparent non-linear relationship between f_E and $T_c - T_a$ is likely due to covariance between f_E, r_H, and Q_a on seasonal and diurnal time scales. The model validation accounted for the changing values of f_E, r_H, and Q_a, and it demonstrated strong model performance at both sites (Fig. 2).

3.5.1. Drivers of leaf temperature

Seasonal climatologies of f_E, r_H, and Q_a revealed seasonal changes in the environmental variables that drive $T_c - T_a$. The f_E exhibited the most pronounced seasonal trends and generally tracked the onset of the monsoon. In the riparian woodland, median f_E increased from 0.2 in May to 0.57 in August. In the upland savanna, median f_E remained low in May and June (0.08 and 0.07, respectively) and increased to 0.32 in August. At both sites, r_H exhibited a much less pronounced seasonal trend. Monthly median r_H values ranged from 12.1 to 14.6 sm^{-1} in the riparian woodland and 20.4 to 24.6 sm^{-1} in the upland savanna. Likewise, median monthly Q_a (measured at 12:00 local time) exhibited little seasonal trend and ranged from 604 to 652 Wm^{-2} in the riparian woodland and 501 to 528 Wm^{-2} in the upland savanna. The greater values of Q_a in the riparian woodland are likely due to the greater canopy cover with lower albedo as well as smaller G flux. The median albedos were 9.3% and 15.2% in the riparian woodland and upland savanna, respectively. The median G fluxes were 59 Wm^{-2} and 119 Wm^{-2}, respectively.

Table 1
Spearman rank correlations between observed Q_a, r_H, and f_E and environmental variables measured by the flux towers, including shortwave insolation (SW↓), vapor pressure deficit (VPD), wind speed (u), and soil water content (SWC) for the riparian woodland and upland savanna.

	Riparian woodland				Upland savanna			
	SW↓	VPD	u	SWC	SW↓	VPD	u	SWC
f_E	−0.39	−0.15	−0.36	0.02	−0.36	−0.34	−0.40	0.76
r_H	−0.15	−0.21	−0.73	0.12	−0.08	−0.02	−0.66	0.04
Q_a	0.86	0.27	0.15	−0.02	0.91	0.20	0.27	0.07

The r_H term can also be calculated directly from temperature measurements by inverting Eq. (5) (Verhoef et al., 1997). The inversion method yielded a different seasonal trend, indicating that r_H decreased throughout the growing season. However, the values of r_H were generally similar using both methods (Supplementary Figure 7).

Spearman rank correlation was used to quantify the sensitivity of observed T_c to the individual variables that drive T_c, including T_a, Q_a, r_H, and f_E. As expected, T_a was highly correlated with T_c in all months at both sites ($r_s \geq 0.75$; Supplementary Figure 8). We controlled for T_a by repeating the analysis with $T_c - T_a$ values. There were coherent seasonal trends in the correlations between $T_c - T_a$ and Q_a, r_H, and f_E at both sites (Fig. 7). In the riparian woodland, $T_c - T_a$ was highly correlated with f_E early in the growing season ($r_s = -0.79$ in May), but the sensitivity to f_E decreased as monsoonal moisture accumulated in the ecosystem ($r_s = -0.14$ in September). The sensitivity to Q_a peaked in the middle of the summer ($r_s = 0.71$ in July) and was lower at the beginning and end of the growing season. The sensitivity to modeled r_H was negligible in all months ($r_s \leq 0.1$). In the upland savanna, $T_c - T_a$ was more sensitive to Q_a in May and June ($r_s = 0.56$ and 0.58, respectively) and more sensitive to f_E after the onset of the monsoon in July. The sensitivity to f_E peaked in July ($r_s = -0.68$) and decreased at the end of the growing season. The sensitivity to modeled r_H was weak in all months ($-0.15 \leq r_s \leq 0.09$).

Spearman rank correlation was also used to quantify the sensitivity of observed Q_a, r_H, and f_E to environmental variables measured by the flux towers, including SW↓, VPD, u, and SWC. The f_E term was negatively correlated with SW↓ and VPD at both sites (Table 1). The f_E term was also negatively correlated with u, potentially because u often peaks late in the afternoon when VPD is highest. The f_E term was negligibly correlated with SWC in the riparian woodland ($r_s = 0.02$) but strongly correlated with SWC in the upland savanna ($r_s = 0.76$), likely

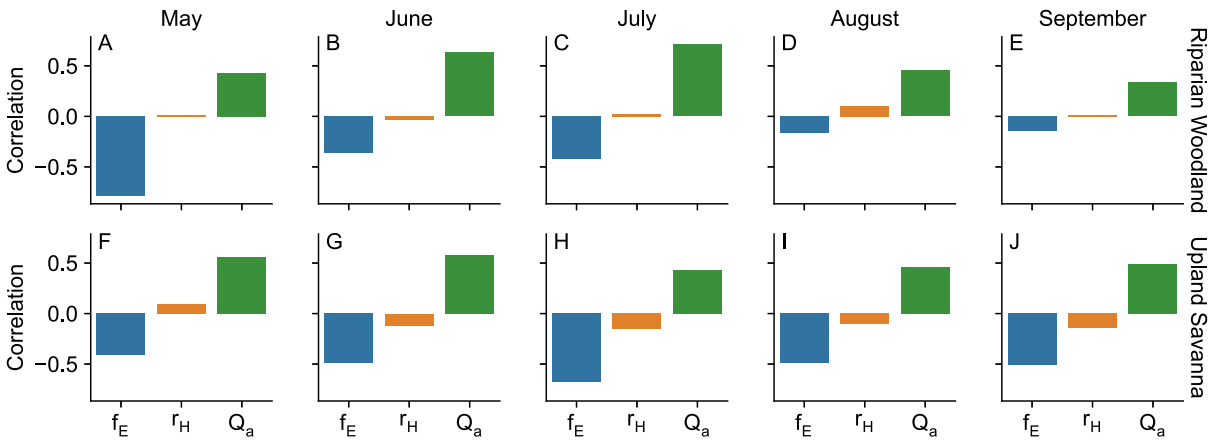

Fig. 7. Spearman rank correlations between $T_c - T_a$ and evaporative fraction (f_E), resistance to sensible heat flux (r_H), and available energy (Q_a) at the riparian woodland (a–e) and upland savanna (f–j). The colored bars represent the correlations for each month of the growing season.

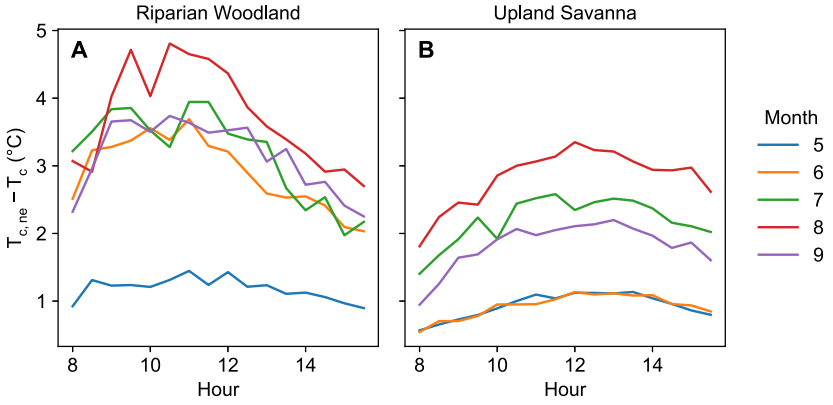

Fig. 8. Diurnal and seasonal climatology of modeled $T_{c,ne} - T_c$, which indicates the change in T_c due to evaporative cooling of the leaf surface. The colored lines represent the mean values for each time of day, grouped by month of the growing season, for the riparian woodland (a) and upland savanna (b).

due to contrasting groundwater availability at the two sites (Mayes et al., 2020; Sabathier et al., 2021). The u term was the dominant driver of r_H at both sites ($r_s = -0.73$ and -0.66, respectively), which was expected given that u is encoded in the r_H calculations. SW↓ was the dominant driver of Q_a ($r_s = 0.86$ and 0.91, respectively). The analysis of the environmental variables also explains the negative correlations between $T_c - T_a$ and r_H at both sites (Fig. 7), which were contrary to expectations. The negative correlations likely emerge from the fact that u has negative correlations with both f_E and r_H (Table 1), yet f_E and r_H have opposing effects on $T_c - T_a$. Thus, the effect of u on f_E and $T_c - T_a$ is likely large enough to confound the relationship between r_H and $T_c - T_a$.

3.6. Evaporative cooling

The modeled values of T_c and $T_{c,ne}$ revealed the change in T_c that can be attributed to evaporative cooling of the canopy. The $T_{c,ne} - T_c$ values were generally greater in the riparian woodland than the upland savanna (Fig. 8). At both sites, seasonal variability in $T_{c,ne} - T_c$ tracked the seasonal trends of f_E. The smallest values of $T_{c,ne} - T_c$ occurred in May at the riparian woodland and in May and June at the upland savanna. The largest values of $T_{c,ne} - T_c$ (i.e., the most evaporative cooling) occurred in August at both sites. In the riparian woodland, the maximum daily climatological $T_{c,ne} - T_c$ was 1.45 °C in May and 4.81 °C in August. In the upland savanna, the maximum daily climatological $T_{c,ne} - T_c$ was 1.14 °C in May and 3.35 °C in August. The dip in $T_{c,ne} - T_c$ values in the middle of the morning is likely a measurement or modeling artifact, potentially caused by shading of the flux tower sensors.

3.7. Impact of evaporative cooling on leaf respiration

Leaf light respiration ($R_{L,light}$) was predicted using modeled values of T_c and $T_{c,ne}$. The difference between the two predictions (ΔR_L) indicates the change in $R_{L,light}$ that is attributable to evaporative cooling of the canopy. In the riparian woodland, ΔR_L exhibited consistent seasonal patterns each year, with the lowest values occurring during the pre-monsoon period in May and the largest values occurring in August (Fig. 9). In May, evaporative cooling decreased $R_{L,light}$ by 5%–11%. In August, evaporative cooling decreased $R_{L,light}$ by 21%–24%. In the upland savanna, ΔR_L varied much more sporadically, likely due to the dependence of the ecosystem on water inputs from precipitation. The smallest values of ΔR_L typically occurred in May and June of each year, and the largest values typically occurred in August. In May, evaporative cooling decreased $R_{L,light}$ by 4%–11%. In August, evaporative cooling decreased $R_{L,light}$ by 7%–28%. The largest value of ΔR_L occurred in July 2008, when evaporative cooling decreased $R_{L,light}$ by 31%. It is important to note the difference in sample size at the two study sites (3 years for the riparian woodland vs. 11 years for the upland savanna) due to the limited measurements of $SW\downarrow$, $SW\uparrow$, and $LW\downarrow$ in the riparian woodland, which may account for some of the contrasting variability.

4. Discussion

We have presented a novel model to predict leaf temperature (T_L) as a linearized function of the evaporative fraction (f_E). The model predictions and empirical observations presented here demonstrate

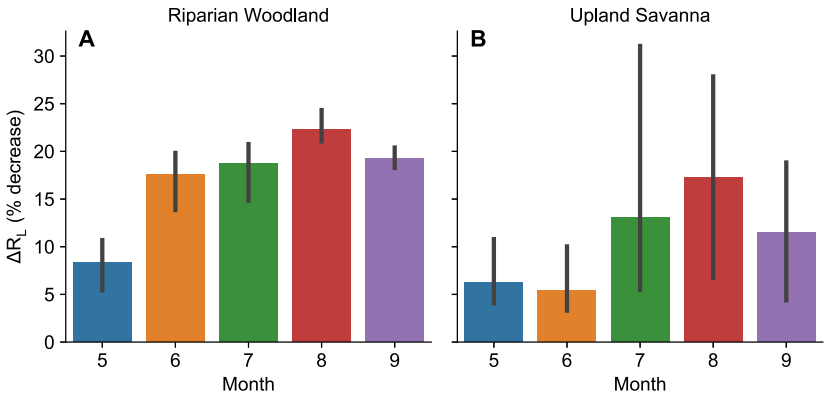

Fig. 9. Monthly mean decrease in daytime leaf respiration (ΔR_L) that is attributable to evaporative cooling for the riparian woodland (a) and upland savanna (b). The black vertical bars indicate the range of monthly mean ΔR_L values for individual years. There are 3 years of data for the riparian woodland and 11 years of data for the upland savanna.

that evapotranspiration reduces T_L by consuming energy that would otherwise be partitioned into sensible heat flux. The model predicts that $T_L - T_a$ varies as a linear function of f_E when all other variables are held constant. The model also predicts that $T_L = T_a$ when $f_E = 1$. When $f_E < 1$, T_L theoretically varies as a function of Q_a and r_H. The theoretical predictions from the energy balance model were tested using canopy-scale measurements of leaf temperature (T_c) from two flux towers with contrasting water availability. At both sites, T_c converged to T_a when f_E approached 1. The mechanistic model presented in Eq. (7) exhibited strong model fit at both sites. Our findings are also consistent with a multi-site synthesis reported by Panwar et al. (2020), who demonstrated that the difference between surface temperature and air temperature was negatively correlated with f_E across a variety of ecosystems.

4.1. Environmental controls on T_c

The flux tower observations suggest that water availability plays an important role in regulating f_E and its impact on T_c. The riparian woodland has consistent access to shallow groundwater (depth to groundwater $\approx$ 10 m), which provides a persistent source of water that is decoupled from the local precipitation regime on short time scales. The upland savanna does not have access to groundwater (depth to groundwater > 100 m) and is thus reliant on water inputs from monsoonal precipitation during the growing season. As a result, f_E was decoupled from near-surface SWC in the riparian woodland (r_s = 0.02) but strongly coupled to SWC in the upland savanna (r_s = 0.76). The enhanced water availability in the riparian woodland resulted in an earlier increase in f_E in the late spring and higher values of f_E throughout the growing season compared to the upland savanna (Fig. 6).

The differences in f_E at the two sites resulted in different magnitudes of evaporative cooling throughout the growing season. In the riparian woodland, $T_c - T_a < 2$ °C for much of the growing season, while in the upland savanna T_c consistently exceeded T_a by as much as 10 °C (Fig. 5). The seasonal patterns of $T_c - T_a$ matched the seasonal patterns in f_E at both sites. That being said, the strength of the correlation between $T_c - T_a$ and f_E in the riparian woodland decreased throughout the growing season, suggesting that Q_a, and not water availability, was the primary driver of riparian T_c by the end of the growing season (Fig. 7). In the upland savanna, $T_c - T_a$ was most strongly correlated with f_E in the middle of the growing season during peak monsoonal precipitation and less strongly correlated with f_E during the drier periods at the beginning and end of the growing season.

At low values of f_E, $T_c - T_a$ is largely regulated by non-evaporative cooling processes (Muller et al., 2021, 2023). The efficiency of non-evaporative cooling is determined by the resistance to sensible heat flux (r_H). At a leaf scale, r_H is a function of leaf size, leaf structure, and the wind speed across the leaf surface (Balding and Cunningham, 1976; Jones, 2014; Leigh et al., 2017). At a canopy scale, r_H is also a function of vegetation cover and vegetation structure, which drive turbulent mixing (Yang and Friedl, 2003; Rigden et al., 2018). The upland savanna experienced a larger range of $T_c - T_a$ values at low values of f_E because there was a larger range of r_H values under those conditions. In the riparian woodland, f_E and r_H covaried more strongly, resulting in a smaller range of $T_c - T_a$ values at low values of f_E. Interestingly, the upland savanna experienced higher wind speeds and likely had smaller leaves (Stromberg et al., 1993), which are typically associated with more efficient heat transfer, but the riparian woodland had lower modeled values of r_H. This suggests that turbulent mixing at a canopy scale played an important role in regulating r_H, which is consistent with previous analyses of r_H across different vegetation types (Rigden et al., 2018; Young et al., 2021).

4.2. Limited homeothermy

The mechanistic relationship between T_L and T_a has received considerable attention in literature (Cavaleri, 2020, and references therein), with various studies arguing that plants exhibit either limited homeothermy ($T_L < T_a$ at high values of T_a), poikilothermy ($T_L \cong T_a$), or megathermy ($T_L > T_a$ at high values of T_a). We found that the riparian woodland generally exhibited poikilothermy. The slope of the relationship between T_c and T_a was close to 1 (β = 0.92) and there were few observations where $T_c < T_a$, even at high values of T_a. The upland savanna exhibited megathermy; the slope of the relationship between T_c and T_a was greater than 1 (β = 1.17) and T_c consistently exceeded T_a. Neither site in this study exhibited a clear signal of limited homeothermy. Moreover, the mechanistic model of T_L always predicts that $T_L \geq T_a$ when $Q_a \geq 0$ W m^{-2} and $f_E \leq 1$. Even if stomatal conductance is not limiting, there is by definition not enough Q_a in the system to increase λE to levels that result in $T_L < T_a$ under normal conditions. It follows from Eq. (6) that $T_L < T_a$ can only occur if $f_E > 1$. Previous studies have demonstrated that $f_E > 1$ only occurs briefly around sunrise and sunset when H is negative and λE is positive, a time of day when the magnitudes of energy fluxes are small. The value of f_E is somewhat constant during daylight hours and typically substantially less than 1 (Crago, 1996; Gentine et al., 2007, 2011). Conditions where $f_E > 1$ can also occur as a result of the "oasis effect" whereby the advection of dry air over well-watered vegetation creates a land-atmosphere feedback that causes λE to exceed Q_a (Baldocchi et al., 2016). The oasis effect is most commonly associated with rice paddies and wetlands in semi-arid climates, but it is not clear how often the effect actually occurs (Baldocchi et al., 2016).

Despite the lack of theoretical or empirical support for limited homeothermy in the data examined here, observations where $T_L < T_a$ are commonly reported in literature. Some researchers have suggested

that observations of limited homeothermy are due to systematic errors from certain types of *in situ* sensors (Still et al., 2019b). However, observations where $T_L < T_a$ have also been reported in studies that measure T_L using infrared radiometers (e.g., Idso et al., 1981; Jackson et al., 1981; Kar and Kumar, 2007; Ballester et al., 2013; Blonder et al., 2020). Thus, there is an apparent paradox whereby observations of $T_L < T_a$ seem highly unlikely given fundamental energy balance constraints (Eq. (6)), but are nonetheless common. Blonder and Michaletz (2018) demonstrated from energy balance theory that limited homeothermy can only occur when stomatal conductance is high and r_H is low. Other research has examined non-steady state T_L dynamics, which are not explored here (e.g., Leigh et al., 2017). The relationship between f_E and T_L established by this study represents another novel constraint on leaf thermoregulation via limited homeothermy. Further theoretical and empirical research is needed to constrain the conditions that result in observations where $T_L < T_A$, especially given the substantial disagreement over how frequently leaf thermoregulation actually occurs in nature (e.g., Blonder et al., 2020; Still et al., 2022).

4.3. Plant carbon balance

Constraining the mechanistic relationship between T_L and T_a is of critical importance for modeling ecosystem responses to anthropogenic climate change. Leaf energy balance and T_L serve as fundamental constraints on the selection and adaptation of plant traits (Michaletz et al., 2015, 2016), which are generally assumed to maximize net carbon uptake while controlling for the risk of plant hydraulic failure (Wolf et al., 2016; Sperry et al., 2017; Mencuccini et al., 2019). Previous trait-based research has focused on the role of stomatal conductance in maximizing photosynthetic assimilation via biochemical fixation of carbon (Cowan and Farquhar, 1977; Medlyn et al., 2011). Here we demonstrate that stomatal conductance also alters net carbon uptake via the impact of evaporative cooling on R_L. In both the riparian woodland and upland savanna, evaporative cooling of the leaf surface often reduced R_L by *ca.* 15% in the middle of the growing season. Reduced T_L from evaporative cooling would also be expected to keep T_L closer to the photosynthetic optimum in hot environments, maximizing photosynthetic assimilation (Roden and Pearcy, 1993; Medlyn et al., 2002). For example, Uni et al. (2022) demonstrated that a reduction in T_L from 40 °C to 35 °C would increase photosynthetic assimilation by 42%. Their study analyzed *Acacia tortilis*, a species that is structurally and functionally similar to *P. velutina*. The regulation of T_L by stomatal conductance represents an important linkage between plant water and carbon cycles that has received little attention in literature (but see Michaletz et al., 2015, 2016) and may alter predictions of optimal plant traits and behavior. All other factors held constant, the data examined here suggest that high levels of λE will enhance net carbon uptake by reducing R_L, which may marginally favor high risk-high reward hydraulic strategies in dryland vegetation (e.g., Hultine et al., 2020; Williams et al., 2022).

4.4. Thermal remote sensing

Eq. (7) also provides a physical basis to interpret thermal remote sensing measurements (Mallick et al., 2022). Tower-mounted infrared radiometers are a reliable proxy for airborne and satellite thermal sensors, which can measure surface temperature over broad spatial scales. Thermal remote sensing is widely used to monitor agricultural productivity (Jones et al., 2009; Maes and Steppe, 2012) and manage water resources (Anderson et al., 2012). Our study joins other recent efforts to unify plant traits and thermal measurements, which will likely yield novel insights into ecosystem processes at leaf to global scales (Still et al., 2019a, 2021; Farella et al., 2022).

5. Conclusion

The mechanistic relationships between water, energy, and carbon fluxes at the leaf surface are of considerable importance for predicting the responses of terrestrial ecosystems to anthropogenic climate change. The model presented here constrains the mechanistic relationship between T_L and T_a and provides a framework to quantify evaporative cooling of the leaf surface. Importantly, the model reveals that $T_L - T_a$ varies as a linear function of f_E and that $T_L - T_a = 0$ °C when $f_E = 1$. The model predictions were validated using measurements of canopy-scale leaf temperature (T_c) from two flux towers. Seasonal variability in measured T_c was primarily driven by f_E, although Q_a also played an important role in regulating T_c in well-watered conditions. Neither the model predictions nor the empirical observations provided evidence for regimes where T_L is substantially less than T_a. Future work is needed to understand the conditions that result in empirical observations of $T_L < T_a$ in croplands. Our analysis also reveals that evaporative cooling of the leaf surface has important functional implications for plant carbon cycling. Evaporative cooling substantially reduced R_L at both study sites. The impact of evaporative cooling on R_L may affect predictions of optimal plant traits and behavior under future climate scenarios.

Declaration of competing interest

The authors declare that they have no known competing financial interests or personal relationships that could have appeared to influence the work reported in this paper.

Data availability

Code and data to replicate the analyses are available online.

Manuscript code and data (Original data) (Github)

Acknowledgments

The authors thank Jean Allen and Bryn Morgan for their assistance with this study. The research was supported by grants from NASA, United States (80NSSC21K1639), the U.S. National Science Foundation (BCS-1660490, EAR-1700555, EAR-1700517, DEB-2003205, and IOS-2216855), and the U.S. Department of Defense's Strategic Environmental Research and Development Program (RC18-1006). Funding for the AmeriFlux data portal was provided by the U.S. Department of Energy Office of Science.

Appendix A. Symbols

Symbol	Description	Unit
C	energy balance closure ratio	—
c_p	specific heat capacity of air	J K^{-1} kg^{-1}
λE	latent heat flux	W m^{-2}
f_E	evaporative fraction	—
G	ground heat flux	W m^{-2}
H	sensible heat flux	W m^{-2}
k	one or two-sided leaf model	—
kB^{-1}	empirical parameter	—
LW↓	longwave downwelling radiation	W m^{-2}
LW↑	longwave upwelling radiation	W m^{-2}
Q_a	available energy	W m^{-2}
$Q_{a,f}$	available energy (forced closure)	W m^{-2}
RH	relative humidity	%
R_L	leaf respiration	μ mol CO_2 m^{-2} s^{-1}
R_n	net radiation	W m^{-2}

Symbol	Description	Unit
r_{am}	resistance to momentum transfer	m s^{-1}
r_{bh}	excess resistance	m s^{-1}
r_H	resistance to sensible heat flux	s m^{-1}
r_s	Spearman rank correlation coefficient	—
SW↓	shortwave downwelling radiation	W m^{-2}
SW↑	shortwave upwelling radiation	W m^{-2}
SWC	soil water content	%
T_a	air temperature	° C
T_c	canopy-scale leaf temperature ($T_c \cong T_L$)	° C
$T_{c,ne}$	canopy-scale leaf temperature when $\lambda E = 0$	° C
T_L	leaf temperature	° C/K
T_{ref}	reference leaf temperature	K
T_s	soil temperature	° C
u	wind speed	m s^{-1}
u_*	friction velocity	m s^{-1}
VPD	vapor pressure deficit	kPa
z_{0h}	roughness length for heat	m
z_{0m}	roughness length for momentum	m
ε_L	leaf emissivity	—
κ	Von Kármán constant	—
ρ	density of air	kg m^{-3}
σ	Stefan–Boltzmann constant	W m^{-2} K^{-4}
ψ_h	stability function for heat	—
ψ_m	stability function for momentum	—

Appendix B. Supplementary data

Supplementary material related to this article can be found online at https://doi.org/10.1016/j.agrformet.2023.109560.

References

Allen, R.G., Pereira, L.S., Raes, D., Smith, M., 1998. Crop Evapotranspiration: Guidelines for Computing Crop Water Requirements. Drainage Paper 56, Food and Agriculture Organization of the United Nations, Rome, Italy.

Amthor, J.S., 1994. Scaling CO2-photosynthesis relationships from the leaf to the canopy. Photosynth. Res. 39 (3), 321–350. http://dx.doi.org/10.1007/BF00014590, URL: http://link.springer.com/10.1007/BF00014590.

Anderson, M.C., Allen, R.G., Morse, A., Kustas, W.P., 2012. Use of Landsat thermal imagery in monitoring evapotranspiration and managing water resources. Remote Sens. Environ. 122, 50–65. http://dx.doi.org/10.1016/j.rse.2011.08.025, URL: https://linkinghub.elsevier.com/retrieve/pii/S0034425712000326.

Atkin, O.K., Bloomfield, K.J., Reich, P.B., Tjoelker, M.G., Asner, G.P., Bonal, D., Bönisch, G., Bradford, M.G., Cernusak, L.A., Cosio, E.G., Creek, D., Crous, K.Y., Domingues, T.F., Dukes, J.S., Egerton, J.J.G., Evans, J.R., Farquhar, G.D., Fyllas, N.M., Gauthier, P.P.G., Gloor, E., Gimeno, T.E., Griffin, K.L., Guerrieri, R., Heskel, M.A., Huntingford, C., Ishida, F.Y., Kattge, J., Lambers, H., Liddell, M.J., Lloyd, J., Lusk, C.H., Martin, R.E., Maksimov, A.P., Maximov, T.C., Malhi, Y., Medlyn, B.E., Meir, P., Mercado, L.M., Mirotchnick, N., Ng, D., Niinemets, Ü., O'Sullivan, O.S., Phillips, O.L., Poorter, L., Poot, P., Prentice, I.C., Salinas, N., Rowland, L.M., Ryan, M.G., Sitch, S., Slot, M., Smith, N.G., Turnbull, M.H., VanderWel, M.C., Valladares, F., Veneklaas, E.J., Weerasinghe, L.K., Wirth, C., Wright, I.J., Wythers, K.R., Xiang, J., Xiang, S., Zaragoza-Castells, J., 2015. Global variability in leaf respiration in relation to climate, plant functional types and leaf traits. New Phytol. 206 (2), 614–636. http://dx.doi.org/10.1111/nph.13253, URL: https://onlinelibrary.wiley.com/doi/10.1111/nph.13253.

Aubrecht, D.M., Helliker, B.R., Goulden, M.L., Roberts, D.A., Still, C.J., Richardson, A.D., 2016. Continuous, long-term, high-frequency thermal imaging of vegetation: Uncertainties and recommended best practices. Agricult. Forest Meteorol. 228–229, 315–326. http://dx.doi.org/10.1016/j.agrformet.2016.07.017, URL: https://linkinghub.elsevier.com/retrieve/pii/S0168192316303434.

Balding, F.R., Cunningham, G.L., 1976. A comparison of heat transfer characteristics of simple and pinnate leaf models. Botanical Gazette 137 (1), 65–74. http://dx.doi.org/10.1086/336843, URL: https://www.journals.uchicago.edu/doi/10.1086/336843.

Baldocchi, D., Knox, S., Dronova, I., Verfaillie, J., Oikawa, P., Sturtevant, C., Matthes, J.H., Detto, M., 2016. The impact of expanding flooded land area on the annual evaporation of rice. Agricult. Forest Meteorol. 223, 181–193. http://dx.doi.org/10.1016/j.agrformet.2016.04.001, URL: https://linkinghub.elsevier.com/retrieve/pii/S0168192316302155.

Ballester, C., Jiménez-Bello, M., Castel, J., Intrigliolo, D., 2013. Usefulness of thermography for plant water stress detection in citrus and persimmon trees. Agricult. Forest Meteorol. 168, 120–129. http://dx.doi.org/10.1016/j.agrformet.2012.08.005, URL: https://linkinghub.elsevier.com/retrieve/pii/S0168192312002572.

Blonder, B., Escobar, S., Kapás, R.E., Michaletz, S.T., 2020. Low predictability of energy balance traits and leaf temperature metrics in desert, montane and alpine plant communities. In: Perez Carmona, C. (Ed.), Funct. Ecol. 34 (9), 1882–1897. http://dx.doi.org/10.1111/1365-2435.13643, URL: https://onlinelibrary.wiley.com/doi/10.1111/1365-2435.13643.

Blonder, B., Michaletz, S.T., 2018. A model for leaf temperature decoupling from air temperature. Agricult. Forest Meteorol. 262, 354–360. http://dx.doi.org/10.1016/j.agrformet.2018.07.012, URL: https://linkinghub.elsevier.com/retrieve/pii/S0168192318302338.

Bonan, G.B., 2016. Ecological Climatology: Concepts and Applications, third ed. Cambridge University Press, New York, NY, USA.

Cavaleri, M.A., 2020. Cold-blooded forests in a warming world. New Phytol. 228 (5), 1455–1457. http://dx.doi.org/10.1111/nph.16916, URL: https://onlinelibrary.wiley.com/doi/10.1111/nph.16916.

Cook, A.M., Berry, N., Milner, K.V., Leigh, A., 2021. Water availability influences thermal safety margins for leaves. Funct. Ecol. 35 (10), 2179–2189. http://dx.doi.org/10.1111/1365-2435.13868, URL: https://onlinelibrary.wiley.com/doi/10.1111/1365-2435.13868.

Cowan, I.R., Farquhar, G.D., 1977. Stomatal function in relation to leaf metabolism and environment: Stomatal function in the regulation of gas exchange. p. 19.

Crago, R.D., 1996. Conservation and variability of the evaporative fraction during the daytime. J. Hydrol. 180 (1–4), 173–194. http://dx.doi.org/10.1016/0022-1694(95)02903-6, URL: https://linkinghub.elsevier.com/retrieve/pii/0022169495029036.

De Kauwe, M.G., Medlyn, B.E., Pitman, A.J., Drake, J.E., Ukkola, A., Griebel, A., Pendall, E., Prober, S., Roderick, M., 2019. Examining the evidence for decoupling between photosynthesis and transpiration during heat extremes. Biogeosciences 16 (4), 903–916. http://dx.doi.org/10.5194/bg-16-903-2019, URL: https://bg.copernicus.org/articles/16/903/2019/.

Drake, J.E., Harwood, R., Va, A., Reich, P.B., Barton, C.V.M., Tjoelker, M.G., 2020. No evidence of homeostatic regulation of leaf temperature in Eucalyptus parramattensis trees: Integration of CO2 flux and oxygen isotope methodologies. New Phytol. 1511–1523. http://dx.doi.org/10.1111/nph.16733.

Drake, J.E., Tjoelker, M.G., Vårhammar, A., Medlyn, B.E., Reich, P.B., Leigh, A., Pfautsch, S., Blackman, C.J., López, R., Aspinwall, M.J., Crous, K.Y., Duursma, R.A., Kumarathunge, D., De Kauwe, M.G., Jiang, M., Nicotra, A.B., Tissue, D.T., Choat, B., Atkin, O.K., Barton, C.V.M., 2018. Trees tolerate an extreme heatwave via sustained transpirational cooling and increased leaf thermal tolerance. Global Change Biol. 24 (6), 2390–2402. http://dx.doi.org/10.1111/gcb.14037, URL: https://onlinelibrary.wiley.com/doi/10.1111/gcb.14037.

Farella, M.M., Fisher, J.B., Jiao, W., Key, K.B., Barnes, M.L., 2022. Thermal remote sensing for plant ecology from leaf to globe. J. Ecology 1365–2745.13957. http://dx.doi.org/10.1111/1365-2745.13957, URL: https://onlinelibrary.wiley.com/doi/10.1111/1365-2745.13957.

Gentine, P., Entekhabi, D., Chehbouni, A., Boulet, G., Duchemin, B., 2007. Analysis of evaporative fraction diurnal behaviour. Agricult. Forest Meteorol. 143 (1–2), 13–29. http://dx.doi.org/10.1016/j.agrformet.2006.11.002, URL: https://linkinghub.elsevier.com/retrieve/pii/S016819230600339X.

Gentine, P., Entekhabi, D., Polcher, J., 2011. The diurnal behavior of evaporative fraction in the soil–vegetation–atmospheric boundary layer continuum. J. Hydrometeorol. 12 (6), 1530–1546. http://dx.doi.org/10.1175/2011JHM1261.1, URL: http://journals.ametsoc.org/doi/10.1175/2011JHM1261.1.

Grossiord, C., Buckley, T.N., Cernusak, L.A., Novick, K.A., Poulter, B., Siegwolf, R.T.W., Sperry, J.S., McDowell, N.G., 2020. Plant responses to rising vapor pressure deficit. New Phytol. 226 (6), 1550–1566. http://dx.doi.org/10.1111/nph.16485, URL: https://onlinelibrary.wiley.com/doi/10.1111/nph.16485.

Harris, C.R., Millman, K.J., van der Walt, S.J., Gommers, R., Virtanen, P., Cournapeau, D., Wieser, E., Taylor, J., Berg, S., Smith, N.J., Kern, R., Picus, M., Hoyer, S., van Kerkwijk, M.H., Brett, M., Haldane, A., del Río, J.F., Wiebe, M., Peterson, P., Gérard-Marchant, P., Sheppard, K., Reddy, T., Weckesser, W., Abbasi, H., Gohlke, C., Oliphant, T.E., 2020. Array programming with NumPy. Nature 585 (7825), 357–362. http://dx.doi.org/10.1038/s41586-020-2649-2, URL: https://www.nature.com/articles/s41586-020-2649-2.

Heskel, M.A., Atkin, O.K., Turnbull, M.H., Griffin, K.L., 2013. Bringing the Kok effect to light: A review on the integration of daytime respiration and net ecosystem exchange. Ecosphere 4 (8), art98. http://dx.doi.org/10.1890/ES13-00120.1, URL: http://doi.wiley.com/10.1890/ES13-00120.1.

Heskel, M.A., O'Sullivan, O.S., Reich, P.B., Tjoelker, M.G., Weerasinghe, L.K., Penillard, A., Egerton, J.J.G., Creek, D., Bloomfield, K.J., Xiang, J., Sinca, F., Stangl, Z.R., Martinez-de la Torre, A., Griffin, K.L., Huntingford, C., Hurry, V., Meir, P., Turnbull, M.H., Atkin, O.K., 2016. Convergence in the temperature response of leaf respiration across biomes and plant functional types. Proc. Natl. Acad. Sci. 113 (14), 3832–3837. http://dx.doi.org/10.1073/pnas.1520282113, URL: https://pnas.org/doi/full/10.1073/pnas.1520282113.

Higgins, R.W., Yao, Y., Wang, X.L., 1997. Influence of the north American monsoon system on the U.S. summer precipitation regime. J. Clim. 10 (10), 2600–2622. http://dx.doi.org/10.1175/1520-0442(1997)010<2600:IOTNAM>2.0.CO;2.

Hong, J., Kim, J., Byun, Y.H., 2012. Uncertainty in carbon exchange modelling in a forest canopy due to kB-1 parametrizations on carbon exchange modelling. Q. J. R. Meteorol. Soc. 138 (664), 699–706. http://dx.doi.org/10.1002/qj.944, URL: https://onlinelibrary.wiley.com/doi/10.1002/qj.944.

Hultine, K.R., Froend, R., Blasini, D., Bush, S.E., Karlinski, M., Koepke, D.F., 2020. Hydraulic traits that buffer deep-rooted plants from changes in hydrology and climate. Hydrol. Process. 34 (2), 209–222. http://dx.doi.org/10.1002/hyp.13587, URL: https://onlinelibrary.wiley.com/doi/10.1002/hyp.13587.

Huntington, J.L., Hegewisch, K.C., Daudert, B., Morton, C.G., Abatzoglou, J.T., McEvoy, D.J., Erickson, T., 2017. Climate engine: Cloud computing and visualization of climate and remote sensing data for advanced natural resource monitoring and process understanding. Bull. Am. Meteorol. Soc. 98 (11), 2397–2410. http://dx.doi.org/10.1175/BAMS-D-15-00324.1, URL: https://journals.ametsoc.org/doi/10.1175/BAMS-D-15-00324.1.

Idso, S., Jackson, R., Pinter, P., Reginato, R., Hatfield, J., 1981. Normalizing the stress-degree-day parameter for environmental variability. Agric. Meteorol. 24, 45–55. http://dx.doi.org/10.1016/0002-1571(81)90032-7, URL: https://linkinghub.elsevier.com/retrieve/pii/0002157181900327.

Jackson, R.D., Idso, S.B., Reginato, R.J., Pinter, P.J., 1981. Canopy temperature as a crop water stress indicator. Water Resour. Res. 17 (4), 1133–1138. http://dx.doi.org/10.1029/WR017i004p01133, URL: http://doi.wiley.com/10.1029/WR017i004p01133.

Jones, H.G., 2014. Plants and Microclimate: A Quantitative Approach to Environmental Plant Physiology, third ed. Cambridge University Press, Cambridge ; New York.

Jones, H.G., Serraj, R., Loveys, B.R., Xiong, L., Wheaton, A., Price, A.H., 2009. Thermal infrared imaging of crop canopies for the remote diagnosis and quantification of plant responses to water stress in the field. Funct. Plant Biol. 36 (11), 978. http://dx.doi.org/10.1071/FP09123, URL: http://www.publish.csiro.au/?paper=FP09123.

Kar, G., Kumar, A., 2007. Surface energy fluxes and crop water stress index in groundnut under irrigated ecosystem. Agricult. Forest Meteorol. 146 (1–2), 94–106. http://dx.doi.org/10.1016/j.agrformet.2007.05.008, URL: https://linkinghub.elsevier.com/retrieve/pii/S016819230700144X.

Kibler, C.L., Schmidt, E.C., Roberts, D.A., Stella, J.C., Kui, L., Lambert, A.M., Singer, M.B., 2021. A brown wave of riparian woodland mortality following groundwater declines during the 2012–2019 California drought. Environ. Res. Lett. 16 (8), 084030. http://dx.doi.org/10.1088/1748-9326/ac1377, URL: https://iopscience.iop.org/article/10.1088/1748-9326/ac1377.

Knauer, J., Zaehle, S., Medlyn, B.E., Reichstein, M., Williams, C.A., Migliavacca, M., De Kauwe, M.G., Werner, C., Keitel, C., Kolari, P., Limousin, J.-M., Linderson, M.-L., 2018. Towards physiologically meaningful water-use efficiency estimates from eddy covariance data. Global Change Biol. 24 (2), 694–710. http://dx.doi.org/10.1111/gcb.13893, URL: https://onlinelibrary.wiley.com/doi/10.1111/gcb.13893.

Kok, B., 1948. A critical consideration of the quantum yield of Chlorella-Photosynthesis. Enzymologia 13, 1–56.

Krich, C., Mahecha, M.D., Migliavacca, M., De Kauwe, M.G., Griebel, A., Runge, J., Miralles, D.G., 2022. Decoupling between ecosystem photosynthesis and transpiration: A last resort against overheating. Environ. Res. Lett. 17 (4), 044013. http://dx.doi.org/10.1088/1748-9326/ac583e, URL: https://iopscience.iop.org/article/10.1088/1748-9326/ac583e.

Leigh, A., Sevanto, S., Close, J., Nicotra, A., 2017. The influence of leaf size and shape on leaf thermal dynamics: Does theory hold up under natural conditions? Plant Cell Environ. 40 (2), 237–248. http://dx.doi.org/10.1111/pce.12857, URL: https://onlinelibrary.wiley.com/doi/10.1111/pce.12857.

Maes, W.H., Steppe, K., 2012. Estimating evapotranspiration and drought stress with ground-based thermal remote sensing in agriculture: A review. J. Exp. Bot. 63 (13), 4671–4712. http://dx.doi.org/10.1093/jxb/ers165, URL: https://academic.oup.com/jxb/article-lookup/doi/10.1093/jxb/ers165.

Mallick, K., Baldocchi, D., Jarvis, A., Hu, T., Trebs, I., Sulis, M., Bhattarai, N., Bossung, C., Eid, Y., Cleverly, J., Beringer, J., Woodgate, W., Silberstein, R., Hinko-Najera, N., Meyer, W.S., Ghent, D., Szantoi, Z., Boulet, G., Kustas, W.P., 2022. Insights into the aerodynamic versus radiometric surface temperature debate in thermal-based evaporation modeling. Geophys. Res. Lett. 49 (15), http://dx.doi.org/10.1029/2021GL097568, URL: https://onlinelibrary.wiley.com/doi/10.1029/2021GL097568.

Mathias, J.M., Trugman, A.T., 2022. Climate change impacts plant carbon balance, increasing mean future carbon use efficiency but decreasing total forest extent at dry range edges. In: Liu, L. (Ed.), Ecol. Lett. 25 (2), 498–508. http://dx.doi.org/10.1111/ele.13945, URL: https://onlinelibrary.wiley.com/doi/10.1111/ele.13945.

Mauder, M., Foken, T., Cuxart, J., 2020. Surface-energy-balance closure over land: A review. Bound.-Lay. Meteorol. 177 (2–3), 395–426. http://dx.doi.org/10.1007/s10546-020-00529-6, URL: https://link.springer.com/10.1007/s10546-020-00529-6.

Mayes, M., Caylor, K.K., Singer, M.B., Stella, J.C., Roberts, D., Nagler, P., 2020. Climate sensitivity of water use by riparian woodlands at landscape scales. Hydrol. Process. 34 (25), 4884–4903. http://dx.doi.org/10.1002/hyp.13942, URL: https://onlinelibrary.wiley.com/doi/10.1002/hyp.13942.

Medlyn, B.E., Dreyer, E., Ellsworth, D., Forstreuter, M., Harley, P.C., Kirschbaum, M.U.F., Le Roux, X., Montpied, P., Strassemeyer, J., Walcroft, A., Wang, K., Loustau, D., 2002. Temperature response of parameters of a biochemically based model of photosynthesis. II. A review of experimental data: Temperature response of photosynthetic parameters - Review. Plant Cell Environ. 25 (9), 1167–1179. http://dx.doi.org/10.1046/j.1365-3040.2002.00891.x, URL: http://doi.wiley.com/10.1046/j.1365-3040.2002.00891.x.

Medlyn, B.E., Duursma, R.A., Eamus, D., Ellsworth, D.S., Prentice, I.C., Barton, C.V.M., Crous, K.Y., De Angelis, P., Freeman, M., Wingate, L., 2011. Reconciling the optimal and empirical approaches to modelling stomatal conductance. Global Change Biol. 17 (6), 2134–2144. http://dx.doi.org/10.1111/j.1365-2486.2010.02375.x, URL: https://onlinelibrary.wiley.com/doi/10.1111/j.1365-2486.2010.02375.x.

Mencuccini, M., Manzoni, S., Christoffersen, B., 2019. Modelling water fluxes in plants: From tissues to biosphere. New Phytol. 222 (3), 1207–1222. http://dx.doi.org/10.1111/nph.15681, URL: https://onlinelibrary.wiley.com/doi/10.1111/nph.15681.

Michaletz, S.T., Weiser, M.D., McDowell, N.G., Zhou, J., Kaspari, M., Helliker, B.R., Enquist, B.J., 2016. The energetic and carbon economic origins of leaf thermoregulation. Nature Plants 2 (9), 16129. http://dx.doi.org/10.1038/nplants.2016.129, URL: http://www.nature.com/articles/nplants2016129.

Michaletz, S.T., Weiser, M.D., Zhou, J., Kaspari, M., Helliker, B.R., Enquist, B.J., 2015. Plant thermoregulation: Energetics, trait–environment interactions, and carbon economics. Trends Ecol. Evol. 30 (12), 714–724. http://dx.doi.org/10.1016/j.tree.2015.09.006, URL: https://linkinghub.elsevier.com/retrieve/pii/S0169534715002396.

Miller, B.D., Carter, K.R., Reed, S.C., Wood, T.E., Cavaleri, M.A., 2021. Only sun-lit leaves of the uppermost canopy exceed both air temperature and photosynthetic thermal optima in a wet tropical forest. Agricult. Forest Meteorol. 301–302, 108347. http://dx.doi.org/10.1016/j.agrformet.2021.108347, URL: https://linkinghub.elsevier.com/retrieve/pii/S0168192321000307.

Missik, J.E.C., Liu, H., Gao, Z., Huang, M., Chen, X., Arntzen, E., Mcfarland, D.P., Verbeke, B., 2021. Groundwater regulates interannual variations in evapotranspiration in a Riparian semiarid ecosystem. J. Geophys. Res.: Atmos. 126 (7), http://dx.doi.org/10.1029/2020JD033078, URL: https://onlinelibrary.wiley.com/doi/10.1029/2020JD033078.

Monteith, J.L., Unsworth, M.H., 2013. Principles of Environmental Physics: Plants, Animals, and the Atmosphere, fourth ed. Elsevier/Academic Press, Boston, OCLC, ocn858967864.

Muller, J.D., Rotenberg, E., Tatarinov, F., Oz, I., Yakir, D., 2021. Evidence for efficient nonevaporative leaf-to-air heat dissipation in a pine forest under drought conditions. New Phytol. 232 (6), 2254–2266. http://dx.doi.org/10.1111/nph.17742, URL: https://onlinelibrary.wiley.com/doi/10.1111/nph.17742.

Muller, J.D., Rotenberg, E., Tatarinov, F., Oz, I., Yakir, D., 2023. Detailed in situ leaf energy budget permits the assessment of leaf aerodynamic resistance as a key to enhance non-evaporative cooling under drought. Plant Cell Environ. pce.14571. http://dx.doi.org/10.1111/pce.14571, URL: https://onlinelibrary.wiley.com/doi/10.1111/pce.14571.

Nelson, J.A., Carvalhais, N., Cuntz, M., Delpierre, N., Knauer, J., Ogée, J., Migliavacca, M., Reichstein, M., Jung, M., 2018. Coupling water and carbon fluxes to constrain estimates of transpiration: The TEA algorithm. J. Geophys. Res.: Biogeosci. 123 (12), 3617–3632. http://dx.doi.org/10.1029/2018JG004727, URL: https://onlinelibrary.wiley.com/doi/abs/10.1029/2018JG004727.

Nelson, J.A., Perez-Priego, O., Sha, Z., 2020a. Ecosystem Transpiration from FLUXNET. Zenodo, http://dx.doi.org/10.5281/ZENODO.3978408, URL: https://zenodo.org/record/3978408, Version Number: v1.0 Type: dataset.

Nelson, J.A., Pérez-Priego, O., Zhou, S., Poyatos, R., Zhang, Y., Blanken, P.D., Gimeno, T.E., Wohlfahrt, G., Desai, A.R., Gioli, B., Limousin, J.-M., Bonal, D., Paul-Limoges, E., Scott, R.L., Varlagin, A., Fuchs, K., Montagnani, L., Wolf, S., Delpierre, N., Berveiller, D., Gharun, M., Belelli Marchesini, L., Gianelle, D., Šigut, L., Mammarella, I., Siebicke, L., Andrew Black, T., Knohl, A., Hörtnagl, L., Magliulo, V., Besnard, S., Weber, U., Carvalhais, N., Migliavacca, M., Reichstein, M., Jung, M., 2020b. Ecosystem transpiration and evaporation: Insights from three water flux partitioning methods across FLUXNET sites. Global Change Biol. 26 (12), 6916–6930. http://dx.doi.org/10.1111/gcb.15314, URL: https://onlinelibrary.wiley.com/doi/10.1111/gcb.15314.

O'Sullivan, O.S., Heskel, M.A., Reich, P.B., Tjoelker, M.G., Weerasinghe, L.K., Penillard, A., Zhu, L., Egerton, J.J.G., Bloomfield, K.J., Creek, D., Bahar, N.H.A., Griffin, K.L., Hurry, V., Meir, P., Turnbull, M.H., Atkin, O.K., 2017. Thermal limits of leaf metabolism across biomes. Global Change Biol. 23 (1), 209–223. http://dx.doi.org/10.1111/gcb.13477, URL: https://onlinelibrary.wiley.com/doi/10.1111/gcb.13477.

Panwar, A., Renner, M., Kleidon, A., 2020. Imprints of evaporative conditions and vegetation type in diurnal temperature variations. Hydrol. Earth Syst. Sci. 24 (10), 4923–4942. http://dx.doi.org/10.5194/hess-24-4923-2020, URL: https://hess.copernicus.org/articles/24/4923/2020/.

Pau, S., Detto, M., Kim, Y., Still, C.J., 2018. Tropical forest temperature thresholds for gross primary productivity. Ecosphere 9 (7), http://dx.doi.org/10.1002/ecs2.2311, URL: https://onlinelibrary.wiley.com/doi/10.1002/ecs2.2311.

PRISM Climate Group, 2021. Monthly Climate Data. Oregon State University, URL: https://prism.oregonstate.edu.

Reich, P.B., Walters, M.B., Ellsworth, D.S., Vose, J.M., Volin, J.C., Gresham, C., Bowman, W.D., 1998. Relationships of leaf dark respiration to leaf nitrogen, specific leaf area and leaf life-span: A test across biomes and functional groups. Oecologia 114 (4), 471–482. http://dx.doi.org/10.1007/s004420050471, URL: http://link.springer.com/10.1007/s004420050471.

Rigden, A., Li, D., Salvucci, G., 2018. Dependence of thermal roughness length on friction velocity across land cover types: A synthesis analysis using AmeriFlux data. Agricult. Forest Meteorol. 249, 512–519. http://dx.doi.org/10.1016/j.agrformet.2017.06.003, URL: https://linkinghub.elsevier.com/retrieve/pii/S0168192317302022.

Roden, J.S., Pearcy, R.W., 1993. The effect of flutter on the temperature of poplar leaves and its implications for carbon gain. Plant Cell Environ. 16 (5), 571–577. http://dx.doi.org/10.1111/j.1365-3040.1993.tb00905.x, URL: https://onlinelibrary.wiley.com/doi/10.1111/j.1365-3040.1993.tb00905.x.

Sabathier, R., Singer, M.B., Stella, J.C., Roberts, D.A., Caylor, K.K., 2021. Vegetation responses to climatic and geologic controls on water availability in southeastern Arizona. Environ. Res. Lett. 16 (6), 064029. http://dx.doi.org/10.1088/1748-9326/abfe8c, URL: https://iopscience.iop.org/article/10.1088/1748-9326/abfe8c.

Salisbury, F.B., Spomer, G.G., 1964. Leaf temperatures of alpine plants in the field. Planta 60 (5), 497–505. http://dx.doi.org/10.1007/BF01894807, URL: http://link.springer.com/10.1007/BF01894807.

Scott, R.L., 2010. Using watershed water balance to evaluate the accuracy of eddy covariance evaporation measurements for three semiarid ecosystems. Agricult. Forest Meteorol. 150 (2), 219–225. http://dx.doi.org/10.1016/j.agrformet.2009.11.002, URL: https://linkinghub.elsevier.com/retrieve/pii/S0168192309002512.

Scott, R.L., 2021a. AmeriFlux BASE US-CMW Charleston Mesquite woodland, ver. 1-5. http://dx.doi.org/10.17190/AMF/1660339.

Scott, R.L., 2021b. AmeriFlux BASE US-SRM Santa Rita Mesquite, Ver. 22-5. http://dx.doi.org/10.17190/AMF/1246104.

Scott, R.L., Edwards, E.A., Shuttleworth, W., Huxman, T.E., Watts, C., Goodrich, D.C., 2004. Interannual and seasonal variation in fluxes of water and carbon dioxide from a riparian woodland ecosystem. Agricult. Forest Meteorol. 122 (1–2), 65–84. http://dx.doi.org/10.1016/j.agrformet.2003.09.001, URL: https://linkinghub.elsevier.com/retrieve/pii/S0168192303002211.

Scott, R.L., Jenerette, G.D., Potts, D.L., Huxman, T.E., 2009. Effects of seasonal drought on net carbon dioxide exchange from a woody-plant-encroached semiarid grassland. J. Geophys. Res. 114 (G4), G04004. http://dx.doi.org/10.1029/2008JG000900, URL: http://doi.wiley.com/10.1029/2008JG000900.

Scott, R.L., Knowles, J.F., Nelson, J.A., Gentine, P., Li, X., Barron-Gafford, G., Bryant, R., Biederman, J.A., 2021. Water availability impacts on evapotranspiration partitioning. Agricult. Forest Meteorol. 297, 108251. http://dx.doi.org/10.1016/j.agrformet.2020.108251, URL: https://linkinghub.elsevier.com/retrieve/pii/S0168192320303531.

Sellers, P., Berry, J., Collatz, G., Field, C., Hall, F., 1992. Canopy reflectance, photosynthesis, and transpiration. III. A reanalysis using improved leaf models and a new canopy integration scheme. Remote Sens. Environ. 42 (3), 187–216. http://dx.doi.org/10.1016/0034-4257(92)90102-P, URL: https://linkinghub.elsevier.com/retrieve/pii/003442579290102P.

Seyednasrollah, B., Young, A.M., Hufkens, K., Milliman, T., Friedl, M.A., Frolking, S., Richardson, A.D., 2019. Tracking vegetation phenology across diverse biomes using Version 2.0 of the PhenoCam Dataset. Sci. Data 6 (1), 222. http://dx.doi.org/10.1038/s41597-019-0229-9, URL: http://www.nature.com/articles/s41597-019-0229-9.

Singer, M.B., Michaelides, K., 2017. Deciphering the expression of climate change within the Lower Colorado River basin by stochastic simulation of convective rainfall. Environ. Res. Lett. 12 (10), 104011. http://dx.doi.org/10.1088/1748-9326/aa8e50, URL: https://iopscience.iop.org/article/10.1088/1748-9326/aa8e50.

Sperry, J.S., Venturas, M.D., Anderegg, W.R.L., Mencuccini, M., Mackay, D.S., Wang, Y., Love, D.M., 2017. Predicting stomatal responses to the environment from the optimization of photosynthetic gain and hydraulic cost: A stomatal optimization model. Plant Cell Environ. 40 (6), 816–830. http://dx.doi.org/10.1111/pce.12852, URL: https://onlinelibrary.wiley.com/doi/10.1111/pce.12852.

Still, C.J., Page, G., Rastogi, B., Griffith, D.M., Aubrecht, D.M., Kim, Y., Burns, S.P., Hanson, C.V., Kwon, H., Hawkins, L., Meinzer, F.C., Sevanto, S., Roberts, D., Goulden, M., Pau, S., Detto, M., Helliker, B., Richardson, A.D., 2022. No evidence of canopy-scale leaf thermoregulation to cool leaves below air temperature across a range of forest ecosystems. Proc. Natl. Acad. Sci. 119 (38), e2205682119. http://dx.doi.org/10.1073/pnas.2205682119, URL: https://pnas.org/doi/full/10.1073/pnas.2205682119.

Still, C., Powell, R., Aubrecht, D., Kim, Y., Helliker, B., Roberts, D., Richardson, A.D., Goulden, M., 2019a. Thermal imaging in plant and ecosystem ecology: Applications and challenges. Ecosphere 10 (6), http://dx.doi.org/10.1002/ecs2.2768, URL: https://onlinelibrary.wiley.com/doi/abs/10.1002/ecs2.2768.

Still, C.J., Rastogi, B., Page, G.F.M., Griffith, D.M., Sibley, A., Schulze, M., Hawkins, L., Pau, S., Detto, M., Helliker, B.R., 2021. Imaging canopy temperature: Shedding (thermal) light on ecosystem processes. New Phytol. 230 (5), 1746–1753. http://dx.doi.org/10.1111/nph.17321, URL: https://onlinelibrary.wiley.com/doi/10.1111/nph.17321.

Still, C.J., Sibley, A., Page, G., Meinzer, F.C., Sevanto, S., 2019b. When a cuvette is not a canopy: A caution about measuring leaf temperature during gas exchange measurements. Agricult. Forest Meteorol. 279, 107737. http://dx.doi.org/10.1016/j.agrformet.2019.107737, URL: https://linkinghub.elsevier.com/retrieve/pii/S0168192319303533.

Stoy, P.C., El-Madany, T.S., Fisher, J.B., Gentine, P., Gerken, T., Good, S.P., Klosterhalfen, A., Liu, S., Miralles, D.G., Perez-Priego, O., Rigden, A.J., Skaggs, T.H., Wohlfahrt, G., Anderson, R.G., Coenders-Gerrits, A.M.J., Jung, M., Maes, W.H., Mammarella, I., Mauder, M., Migliavacca, M., Nelson, J.A., Poyatos, R., Reichstein, M., Scott, R.L., Wolf, S., 2019. Reviews and syntheses: Turning the challenges of partitioning ecosystem evaporation and transpiration into opportunities. Biogeosciences 16 (19), 3747–3775. http://dx.doi.org/10.5194/bg-16-3747-2019, URL: https://bg.copernicus.org/articles/16/3747/2019/.

Stoy, P.C., Mauder, M., Foken, T., Marcolla, B., Boegh, E., Ibrom, A., Arain, M.A., Arneth, A., Aurela, M., Bernhofer, C., Cescatti, A., Dellwik, E., Duce, P., Gianelle, D., van Gorsel, E., Kiely, G., Knohl, A., Margolis, H., McCaughey, H., Merbold, L., Montagnani, L., Papale, D., Reichstein, M., Saunders, M., Serrano-Ortiz, P., Sottocornola, M., Spano, D., Vaccari, F., Varlagin, A., 2013. A data-driven analysis of energy balance closure across FLUXNET research sites: The role of landscape scale heterogeneity. Agricult. Forest Meteorol. 171–172, 137–152. http://dx.doi.org/10.1016/j.agrformet.2012.11.004, URL: https://linkinghub.elsevier.com/retrieve/pii/S0168192312003413.

Stromberg, J., 2013. Root patterns and hydrogeomorphic niches of riparian plants in the American Southwest. J. Arid Environ. 94, 1–9. http://dx.doi.org/10.1016/j.jaridenv.2013.02.004, URL: https://linkinghub.elsevier.com/retrieve/pii/S0140196313000220.

Stromberg, J.C., Wilkins, S.D., Tress, J.A., 1993. Vegetation-hydrology models: Implications for management of Prosopis Velutina (Velvet Mesquite) riparian ecosystems. Ecol. Appl. 3 (2), 307–314. http://dx.doi.org/10.2307/1941833, URL: http://doi.wiley.com/10.2307/1941833.

Thom, A.S., 1972. Momentum, mass and heat exchange of vegetation. Q. J. R. Meteorol. Soc. 98 (415), 124–134. http://dx.doi.org/10.1002/qj.49709841510, URL: https://onlinelibrary.wiley.com/doi/10.1002/qj.49709841510.

Thomas, B.E., Pool, D.R., 2006. Trends in Streamflow of the San Pedro River, Southeastern Arizona, and Regional Trends in Precipitation and Streamflow in Southeastern Arizona and Southwestern New Mexico. Professional Paper 1712, U.S. Geological Survey, Reston, Virginia.

Twine, T., Kustas, W., Norman, J., Cook, D., Houser, P., Meyers, T., Prueger, J., Starks, P., Wesely, M., 2000. Correcting eddy-covariance flux underestimates over a grassland. Agricult. Forest Meteorol. 103 (3), 279–300. http://dx.doi.org/10.1016/S0168-1923(00)00123-4, URL: https://linkinghub.elsevier.com/retrieve/pii/S0168192300001234.

Uni, D., Sheffer, E., Winters, G., Lima, A.C., Fox, H., Klein, T., 2022. Peak photosynthesis at summer midday in Acacia trees growing in a hyper-arid habitat. Trees http://dx.doi.org/10.1007/s00468-022-02344-7, URL: https://link.springer.com/10.1007/s00468-022-02344-7.

Verhoef, A., De Bruin, H., Van Den Hurk, B., 1997. Some practical notes on the parameter kB-1 for sparse vegetation. J. Appl. Meteorol. 36 (5), 560–572, URL: https://www.jstor.org/stable/26182252.

Vinod, N., Slot, M., McGregor, I.R., Ordway, E.M., Smith, M.N., Taylor, T.C., Sack, L., Buckley, T.N., Anderson-Teixeira, K.J., 2022. Thermal sensitivity across forest vertical profiles: Patterns, mechanisms, and ecological implications. New Phytol. nph.18539. http://dx.doi.org/10.1111/nph.18539, URL: https://onlinelibrary.wiley.com/doi/10.1111/nph.18539.

Way, D.A., Holly, C., Bruhn, D., Ball, M.C., Atkin, O.K., 2015. Diurnal and seasonal variation in light and dark respiration in field-grown *Eucalyptus pauciflora*. In: Tissue, D. (Ed.), Tree Physiol. 35 (8), 840–849. http://dx.doi.org/10.1093/treephys/tpv065, URL: https://academic.oup.com/treephys/article-lookup/doi/10.1093/treephys/tpv065.

Williams, J., Stella, J.C., Voelker, S.L., Lambert, A.M., Pelletier, L.M., Drake, J.E., Friedman, J.M., Roberts, D.A., Singer, M.B., 2022. Local groundwater decline exacerbates response of dryland riparian woodlands to climatic drought. Global Change Biol. 28 (22), 6771–6788. http://dx.doi.org/10.1111/gcb.16376, URL: https://onlinelibrary.wiley.com/doi/10.1111/gcb.16376.

Wolf, A., Anderegg, W.R.L., Pacala, S.W., 2016. Optimal stomatal behavior with competition for water and risk of hydraulic impairment. Proc. Natl. Acad. Sci. 113 (46), http://dx.doi.org/10.1073/pnas.1615144113, URL: https://pnas.org/doi/full/10.1073/pnas.1615144113.

Yang, R., Friedl, M.A., 2003. Determination of roughness lengths for heat and momentum over boreal forests. Bound.-Lay. Meteorol. 107 (3), 581–603. http://dx.doi.org/10.1023/A:1022880530523, URL: http://link.springer.com/10.1023/A:1022880530523.

Young, A.M., Friedl, M.A., Seyednasrollah, B., Beamesderfer, E., Carrillo, C.M., Li, X., Moon, M., Arain, M.A., Baldocchi, D.D., Blanken, P.D., Bohrer, G., Burns, S.P., Chu, H., Desai, A.R., Griffis, T.J., Hollinger, D.Y., Litvak, M.E., Novick, K., Scott, R.L., Suyker, A.E., Verfaillie, J., Wood, J.D., Richardson, A.D., 2021. Seasonality in aerodynamic resistance across a range of North American ecosystems. Agricult. Forest Meteorol. 310, 108613. http://dx.doi.org/10.1016/j.agrformet.2021.108613, URL: https://linkinghub.elsevier.com/retrieve/pii/S0168192321002999.